

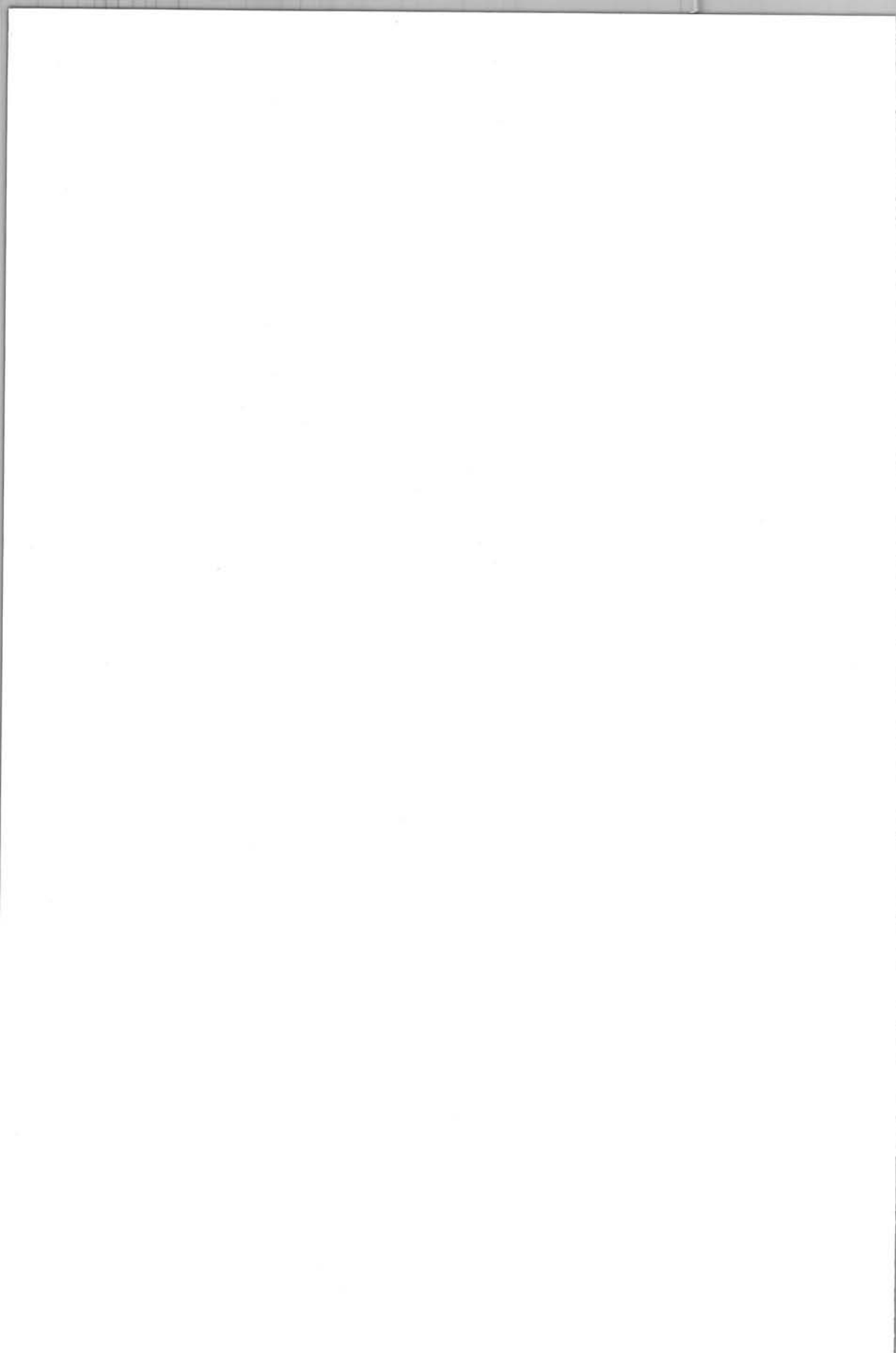
Series 01 Aerodynamics 05

A Review of Propeller Modelling Techniques Based on Euler Methods

G.J.D. Zondervan



Delft University Press



706316

A Review of Propeller Modelling Techniques Based on Euler Methods

Bibliotheek TU Delft



C 3021866

2392
345
0



A Review of Propeller Modelling Techniques Based on Euler Methods

G.J.D. Zondervan



Delft University Press / 1998

Published and distributed by:

Delft University Press
Mekelweg 4
2628 CD Delft
The Netherlands
Telephone +31 (0)15 278 32 54
Fax +31 (0)15 278 16 61
e-mail: DUP@DUP.TUdelft.NL

by order of:

Faculty of Aerospace Engineering
Delft University of Technology
Kluyverweg 1
P.O. Box 5058
2600 GB Delft
The Netherlands
Telephone +31 (0)15 278 14 55
Fax +31 (0)15 278 18 22
e-mail: Secretariaat@LR.TUdelft.NL
website: <http://www.lr.tudelft.nl/>



Cover: Aerospace Design Studio, 66.5 x 45.5 cm, by:
Fer Hakkaart, Dullenbakkersteeg 3, 2312 HP Leiden, The Netherlands
Tel. +31 (0)71 512 67 25

90-407-1568-8

Copyright © 1998 by Faculty of Aerospace Engineering

All rights reserved.

No part of the material protected by this copyright notice may be reproduced or utilized in any form or by any means, electronic or mechanical, including photocopying, recording or by any information storage and retrieval system, without written permission from the publisher: Delft University Press.

Printed in The Netherlands

Contents

1 Introduction	4
1.1 Future propulsion concepts	4
1.2 Introduction in the propeller slipstream interference problem	6
2 Propeller modelling	7
2.1 Propeller aerodynamics	7
2.1.1 Basic layout, onset flow angles and induced velocities	8
2.1.2 Forces acting on propellers	9
2.1.3 Propeller wake	10
2.1.4 Viscous effects in the boundary layer on the blade	12
2.2 Review of classical propeller modelling methods	13
2.2.1 Momentum theories	14
2.2.2 Blade-element theories	16
2.2.3 Vortex theories	16
2.3 Pros and cons of the different theories	20
2.4 Propeller jump conditions for Euler methods	22
3 Introduction into Euler methods	24
3.1 Hierarchy of flow equations	24
3.2 Introduction of the Euler equations	25
3.3 Solution procedure in Euler methods	26
3.3.1 Discretization of the system of equations	26
3.3.2 The concept of numerical viscosity	27
3.3.3 Solution of the discretized system	28
3.4 Initial and boundary conditions for the flow problem	28
3.5 The propeller slipstream as an initial-boundary-value problem.	30
4 Unsteady propeller slipstream modelling	31
4.1 Quasi-steady modelling of propeller slipstreams	32
4.1.1 Transformation of the Euler equations	32
4.1.2 Boundary conditions	34
4.1.3 Initial condition	39
4.2 Modelling of the unsteady flow due to propeller slipstreams	39
4.2.1 Transformation of the Euler equations	39
4.2.2 Grid generation for propeller flows	41
4.2.3 Interface boundary condition between grid blocks	42
4.2.4 Initial condition	43
4.3 Some results of testcases	43
4.4 Wake development as a part of the iteration process	45
5 Propeller simulation by actuator-disc representation	47
5.1 Introduction of actuator disc concept	47
5.2 Boundary conditions	48
5.2.1 Boundary conditions using prescribed work and force	48
5.2.2 Boundary conditions using prescribed flow conditions	50

5.2.3 Addition of source terms to the Euler equations	52
5.3 Comparison of the methods	53
5.4 Simulation of counter rotating propellers	53
6 Conclusions	54
References	56
Figures	61

Summary

Future generation civil aircraft will be powered by new, highly efficient propeller propulsion systems. New, advanced design tools like Euler methods will be needed in the design process of these aircraft. This report describes the application of Euler methods to the modelling of flowfields generated by propellers.

An introduction is given in the general layout of propellers and the propeller slipstream. It is argued that Euler methods can treat a wider range of flow conditions than the classical propeller theories. The power of Euler methods lies in the fact a separate wake model is not needed because their solution includes the propeller slipstream.

Two different ways are described of modelling the propeller slipstream using Euler methods. These are the time-accurate approach that uses the real propeller geometry and the time-averaged approach using an actuator disc representation of the propeller. Both techniques and their specifics concerning the grid and the boundary conditions that have to be imposed are described.

The results of a few propeller calculations using Euler methods are described. Discrepancies between experiments and the simulations can often be traced back to the neglect of the physical viscosity and the quality of the grid. Research is still ongoing into further improving the mathematical flow models and using new concepts like grid adaption.

1 Introduction

A very important subject in the development of the next generation civil aircraft will be the application of highly efficient propulsion systems. Many of these systems use some kind of advanced, high efficiency propellers for generating thrust. The proper integration of these systems in the aircraft design is a very complicated but essential problem to be solved in the design process of new aircraft. The aerodynamic phenomena that occur in the propeller slipstream due to the mutual interference of the propeller, nacelle and lifting surfaces are not yet sufficiently understood and are still the subject of investigation.

This essay deals with the subject of propeller modelling used in the aerodynamic design of aircraft. Emphasis is put on the application of Computational Fluid Dynamics (CFD) in this field. In particular the use of Euler methods for treating the propeller interference problem is described. This because Euler methods form the upper limit in terms of computational expense for routine application with present day computers. No attention is given to other, less 'expensive' methods in CFD like the potential-flow methods. The interested reader is referred to Heyma^[1.1] for this.

In this chapter an introduction is given in the propeller slipstream interference problem. Also the significance of this problem in new propulsion concepts is explained. The operating conditions of new propulsion systems require a more fundamental approach in the aerodynamic design process. In that respect the advantages of Euler methods over other more conventional propeller modelling methods will be dealt with. In Chapter 2, following a basic introduction in the aerodynamics of propellers, a review is presented of some of the classical propeller modelling methods developed until the late 50's. In Chapter 3 a brief introduction is given in the theory behind Euler methods. In Chapter 4 the application of Euler methods to real time-dependent propeller simulation is treated. In Chapter 5 the time-averaged approach is described in which use is made of the actuator-disc model. In both chapters emphasis is put on the different ways of prescribing boundary conditions for the flow problem. Where relevant the results of the different models will be described and compared with each other.

1.1 Future propulsion concepts

In the second half of the 70's, responding to the sharp rise in the fuel prices in the aftermath of the oil crisis, attention was focused on the development of a new generation of highly efficient propulsion systems. These systems would be much more efficient than the turbofan engine of that time. The first results of that investigation resulted in the propfan concept. This engine uses an advanced turbojet as a core combined with propeller blades especially designed for operating at Mach numbers up to 0.8. Compared to conventional turboprop blades the propfan blades are highly loaded and operate locally at transonic speeds. A major

disadvantage of the propfan is the very high level of noise generated by the propeller^[1.2]. This results in the need for extra noise reduction measures for the passenger cabin. The extra weight associated with the noise reduction materials partially overshadows the predicted advantages in fuel savings.

At the same time as the single-blade row propfan the counter-rotating propfan concept emerged. The use of counter-rotating blade rows has some important advantages^[1.3]. It has better aerodynamic efficiency for the same disc loading, a higher permissible disc loading, lesser distortion of the airflow around the wing (in case of a wing-mounted installation), all because the second blade row removes the swirl introduced by the first blade row. On the other hand experimental investigations show that noise levels are not reduced and the characteristic low frequency of the dual propeller configuration noise makes noise reduction even harder. This causes that the design expenses and the weight of the contra-rotating propfan are greater than those of the single-rotation version.

Use of ducted propfans makes an even higher disc loading possible. The ducted propfan is better able to generate a larger static pressure increase over the propeller(s). The duct is used as an exit nozzle to convert the static energy of the flow into flow velocity. The duct can also be used to decelerate the incoming flow to a Mach number at which choking of the propeller, with its adverse effect on the efficiency, is prevented. Consequently, in contrast to the unducted version, the shrouded propfan is not limited to a flight Mach number of 0.75 to 0.8, but can also be used in the region above these values, which is desirable for long-range aircraft. Another interesting prospect of the ducted propfan is its lower sound production.

All in all the fuel saving potential for the propfan-like engines can be quite spectacular. For commercial applications reductions of 15-20% should be possible compared to equivalent turbofan systems. However, although the future of the propfan looked promising, at present the research into propfan technology has been halted. The reason for this is the development and production costs associated with the propfan concept. Following the oil crisis the oil price did not rise as much as was expected. Therefore the extra costs of new and derivative aircraft powered by propfans would make the aircraft too expensive for the airlines. The introduction of the first propfan powered aircraft therefore seems to be postponed until some structural rise in the fuel costs^[1.4].

At present the research in propulsion systems is redirected to the classical turbofan and turboprop engines. Improvements of these engine types are still possible. Some latest trends are the further increase of the bypass ratio of the turbofan (Ultra-High bypass)^[1.5] which will lead to a still higher efficiency and the application of new blade forms for the turboprop which are designed for higher efficiency and lower noise levels. In all it can be said that the detailed investigation of propeller or propeller-like flows and their influence on the airframe remains a very important subject in the aircraft design process. Substantial improvements are to be expected by an integrated design of the propulsion system and the aircraft.

1.2 Introduction in the propeller slipstream interference problem

The airflow passing through the plane of the propeller is influenced not only by the propeller itself but also by the airframe behind it. Therefore the propeller which is installed in an aircraft configuration operates at quite different conditions than an un-installed propeller. The flow around the wing can also be distorted substantially compared to a 'clean' wing. In Chapter 2 a description is given of the induced velocities that determine both the flow in the plane of the propeller and around the nacelle and wing.

Some examples of flow problems resulting from propeller slipstream interaction can be mentioned. First example is the flow around a combination of a supercritical wing and a highly loaded propeller. If the wing is designed for a very specific Mach number to give optimum performance, even a slight Mach number increase can bring the section in the drag-rise area resulting in a much higher drag. Also the swirl of the propeller will lead to a modified lift-distribution that can differ considerably from the optimum (minimum drag) one. Slipstream-induced separation of the boundary layer can also lead to dramatically more drag. A second example of flow problems is the off-design flight handling characteristics of propeller driven aircraft. The stability and control of these aircraft in a landing configuration can be affected in a very negative sense in case of a high propeller loading (large nose-down pitching moments) as well as in the case of an engine malfunction.

The interference effects between propeller and aircraft can thus seriously degrade the performance of the aircraft and the installed propulsion system. In the case of the propfan-like systems, the apparent fuel saving capability of these advanced propulsion systems can only be realized if the engine is integrated properly in the airframe so that undesirable aerodynamic interference effects are eliminated. This interference problem must be analyzed thoroughly to guarantee the performance of the complete aircraft. By proper shaping of the airframe the propeller-body interference can be exploited for drag reduction of the aircraft (or equivalent the increase of the propeller efficiency and thrust). The efficiency can be improved by recovering the energy which is present in the form of swirl in the propeller wake. This can be achieved, up to a certain degree, by the wing and nacelle which form an obstacle for the rotating slipstream. The same idea leads to the application of guide vanes in turbomachinery and by using the already mentioned counter-rotating propellers.

The application of new propulsion systems requires new design codes that are able to capture all the flow features associated with advanced propeller concepts. Due to the complicated geometrical shape of the propeller blades, their transonic working condition and due to the very high blade loading of the advanced propulsion systems, an accurate prediction of the propeller performance is no longer possible with classical propeller modelling methods. Although some of the classical methods are quite sophisticated they completely fail for present day high subsonic propellers. Shockwaves and the complicated vortex structure of the propeller wake are features that prescribe the use of Euler methods. Therefore from Chapter 3 on the application of Euler methods for treating the propeller slipstream interaction problem is described.

2 Propeller modelling

The design of propellers has always been an important topic in aerospace and naval industries. For a long time the specifics about propeller propulsion were unknown. Throughout the 19th century screw-propellers intended for propelling ships were designed largely empirically. Since then much effort has been invested to investigate propeller flows. Propeller flow models have been developed in order to be able to predict the performance and the flow field of propellers and to help design new ones.

The next sections give a survey of propeller modelling techniques that have been developed in the past. The reason of this survey is to provide a background for the recently developed propeller models which are based on these classical theories. Especially the period ranging from the late 1800's to the 1940's is considered during which most of the progress in understanding propeller flows has been made. This was also the period in which major progress was made in the design of propeller driven aircraft. Early methods like the momentum, blade-element and vortex theory were developed in this period. From the 1940's to the 1970's there was considerable less development in the field of propeller modelling because emphasis was put on developing turbofan engines. Only since the 1980's new interest emerged for the subject when propfan propulsion systems were developed aimed at achieving greater fuel efficiency. The advancement of computer technology opened up the avenue for more sophisticated methods based on the potential flow, Euler and the Navier-Stokes equations.

First a basic introduction is given of the general layout of the propeller and its impact on the air flowing through the plane of the propeller. Then the development is reviewed of the propeller modelling development starting with the momentum theory of Froude and finishing with the most complete 'analytical' model that is available, the vortex theory of Theodorsen. The different models are compared with each other and their basic advantages and drawbacks are summarized.

2.1 Propeller aerodynamics

In this section a review is given of the phenomena taking place in the flow field of propellers and propfans. First the layout of the propeller blades and the flow angles that define the operating condition of a propeller are described. The resulting lift and drag forces acting on the propeller are described as is the wake trailing the propeller blades. Non-symmetrical onset flow of the propeller plane and its effects are considered as well. Finally a description is given of the viscous effects occurring in the boundary layer on the propeller blades.

2.1.1 Basic layout, onset flow angles and induced velocities

The basic aim of a propeller is to produce thrust which helps an aircraft to overcome drag forces during flight. Thrust is generated by the addition of momentum to the airflow by the propeller blades. Therefore propeller blades have an airfoil shape which is capable of exerting forces on the flow. In this way the blades of propellers are similar to the wings of an airplane which produce lift to balance the gravitational force. The 'lift' forces generated by the propeller blades are propelling the aircraft. For a sustained propeller motion the drag forces acting on the propeller blades have to be balanced by the power of the engine.

The basic difference between wings and propeller blades is the way in which the velocity vector of the onset flow of the blades is composed. For propellers this vector is the vector sum of the aircraft velocity, the rotational speed of the blade and the velocity induced by the environment (wake, nacelle, wing, other blades). Figure 2.1 illustrates this composition in the case of symmetrical onset flow in front of the propeller. Here vector w is the induced velocity due to the environment. Its axial and tangential components are added to the axial flow velocity V_0 and the rotational velocity ωr . The radial velocity component of w is not considered in Figure 2.1. Usually this component of the induced velocity vector is small and can be ignored because of its limited impact on the blade section characteristics. However, this may not always be the case in the boundary layer on a propeller blade as will be described in Section 2.1.4.

The size and orientation of the velocity vector is varying continuously across the propeller disc. This can be explained by the asymmetry of the aircraft geometry with regard to the propeller axis but other more important causes can be mentioned. They are the asymmetric onset flow of the propeller due to the angle of attack or sideslip of an aircraft and asymmetric onset flow due to the propeller wake in case of high blade loading.

In the case of asymmetric onset flow due to asymmetric flight conditions the flow will have a component normal to the propeller axis. This is illustrated in Figure 2.2 in the case of a propeller at angle of attack. The total velocity vector V (including the induced velocity components) will have a component in the plane of the propeller disc of:

$$V_z = V \sin \alpha_p \quad (2.1)$$

The change of the tangential velocity component depends on the azimuth angle (ϑ) of the blade. The resulting tangential velocity experienced by the blade is:

$$V_t = \omega r + V \sin \alpha_p \sin \vartheta \quad (2.2)$$

This velocity varies with ϑ resulting in a variation of the angle of attack of the blade and asymmetrical blade forces and moments. A similar situation arises in case of sideslip. That problem can be viewed as simply rotating the configuration 90 degrees.

The wake of a lightly loaded propeller, which has an ordered, helical structure, induces a

circumferential velocity distribution in cross-sections parallel to the propeller plane like illustrated in Figure 2.3. The induced velocity distribution in the plane of the propeller results in a in circumferential direction constant but in radial direction varying angle of attack of the sections of a propeller blade. However, if the propeller blades are highly loaded, non-linear effects will arise and the ordered, helical structure of the wake will be destroyed. This results in a continuously varying induced velocity distribution in the propeller plane and therefore in a continuous variation of the angle of attack and loading of the blades during rotation.

Another important source of induced velocities is the close proximity of other blades, the "cascade" effect. This effect is substantial in the blade root area where blade trailing edges and blade leading-edges approach each other. In propeller analysis methods which use 2D aerodynamic section data often use is made of some kind of cascade correction theory. In these theories the flow around the affected airfoil is compared with that of an airfoil in a large row of evenly spaced airfoils (cascade of airfoils). A cascade correction theory can be found in Black ^[2.1]. Interpolation is used for defining cascade correction factors for blade-elements between the root where the effect is maximum and the tip where cascade effects are minimal.

2.1.2 Forces acting on propellers

The forces that act on propellers can be categorized into pressure forces and friction forces. The local angle of attack determines the operating condition of an element of the propeller blade, resulting in a certain pressure distribution around the airfoil. In normal (positive thrust) conditions the pressure is decreased at the upper side of the airfoil (the upstream side of the propeller disc) and increased at the lower side of the airfoil (the downstream side of the propeller disc). Integration of the pressure distribution along the airfoil leads to a resulting section pressure force. Lift and drag components can be derived as well as thrust and torque-force components, see Figure 2.1. Integration of the contribution of all elements along the blade will lead to the total thrust and drag of the blade.

The friction force is the force due to viscous effects in the boundary layer on the propeller blade. The friction force acts in the direction of the local flow on the surface of the blade. Because of centrifugal and Coriolis forces the development of the boundary layer on a propeller blade can be highly three dimensional. In Section 2.1.4 this boundary layer development is described in more detail. An accurate calculation of the friction force will require detailed information of the boundary layer development. Calculation of the boundary layer is not customary in propeller analysis methods. Usually the empirically obtained friction force is thought as acting in the direction of the local flow just outside the boundary layer. Also use is made of experimentally obtained lift and drag coefficients that include both the contributions of the friction and pressure forces.

Because of the finiteness of the propeller blade and the dominating centrifugal force the flow outside the boundary layer cannot be treated 2D in the tip region. The use of two-dimensional airfoil characteristics requires a tip relief scaling of the airfoil characteristics in the tip region. Charts can be used that contain scaling factors for the spanwise distribution of lift and drag due to the lift. These factors are functions of the ratio of blade chord to blade radius, radial location on the blade and the tip Mach number. This method is only valid for straight

propeller blades. If swept blades are used another correction method, the conical flow theory relief model can be used. For specifics about both methods the reader is referred to Egolf et al. [2,2].

2.1.3 Propeller wake

Like a wing, a propeller blade produces a wake trailing the propeller blade, resulting in the so-called propeller slipstream. This slipstream consists of sheets of vorticity originating from the separation of the flow from the trailing edge of the blade. Air flowing through the propeller plane suddenly experiences an increase in static pressure and experiences a tangential acceleration while its axial and radial velocity components remain unchanged. Therefore the wake initially has a helical shape.

The helical shape of the vortex sheets can easily be distorted by the surroundings. In specific situations the helical structure of the wake can even be completely destroyed. The take-off condition can be mentioned in which the forward speed of the aircraft is small and the thrust loading on the blade is high. In this situation the angle of attack of the blade is high resulting in very high vorticity in the slipstream which destroys the helical shape. Also the case can be mentioned in which the propeller is used for thrust reversal. In that case the propeller wake can even be traveling in upstream direction.

Some influences can be mentioned which are known to distort the propeller wake. First of all, the wake is influenced by the forces exerted by the blade. The flow passing the blade is pushed aside and a perturbation velocity is added almost perpendicular to the blade trajectory. This causes the vortex sheet to change shape. It is moving relative to the unperturbed flow. The air in the slipstream between two successive vortex sheets moves along with them. At the outer boundary of the wake the flow outside the wake gives way for the outer edge of the sheets. This results in cross flows at both sides of a sheet, see Figure 2.4.

The shape of the wake is also influenced by self-induction. Because of the vorticity in the wake one part of the wake induces velocities at other parts of the wake. The sense of rotation of the vortex lines is such that (for positive thrust) the fluid in the slipstream has an increased axial velocity and a rotational velocity in the same sense as the rotation of the propeller. Due to the self-induction the tip-end of the vortex sheet rolls up into a tip vortex, see Figure 2.5. This tip vortex has, in general, a strength equal to the maximum circulation strength along the blade. The diameter of the tip vortices is roughly 10% of the blade chord [2,3]. These tip vortices are the dominating structures in a propeller slipstream. At the blade root a similar roll up may occur but the strength of the resulting vortex is much less significant.

Also the expansion of the propeller slipstream can be mentioned. As remarked earlier the propeller increases the pressure at the downstream side of the propeller disc. As the wake moves downstream of the propeller, the flow expands and the static pressure gradually decreases, being transformed into an axial and a circumferential velocity. Finally (far downstream) the velocity increments are about twice their value at the propeller plane, while the static pressure is reduced to its freestream value. This expansion process reduces the diameter of the slipstream tube. This reduction is especially significant for highly loaded

propellers.

Another important subject is the interaction of the propeller wake with a solid body. In Johnston ^[2.3] a description is given of a visualization study of a propeller slipstream interacting with a wing. In Marshall ^{[2.4],[2.5]} some theory is presented regarding the cutting of a vortex which occurs in a propeller slipstream.

Some typical phenomena take place when the propeller tip vortex pass the wing of an aircraft. As the tip vortex moves towards the wing leading-edge it deforms due to an image vortex effect at the wing leading-edge. In Figure 2.6 a vortex filament as well as the wing planform are viewed from top-side down. The mirror image of the vortex is drawn in the inside of the wing. The direction of rotation of the vortex determines the direction of the deformation of the vortex filament along the leading-edge. Then the vortex passes the leading-edge and the vortex filament is cut in two parts. In this cutting process shear forces dominate and therefore the process is highly viscous. During this cutting process the fluid motion in the core of the vortex is suddenly blocked by the wing surface. This means that no axial motion of the fluid is possible as long as the vortex is interrupted by the wing. This process can be compared with the sudden closure of a tap in a line filled with running water. The sudden obstruction will cause the formation of pressure waves on both sides of the wing surface. A so-called vortex shock will form at the wing side where the core fluid of the vortex moves in the direction of the wing surface and an expansion wave will form at the other side. Both waves propagate along the vortex away from the wing ^{[2.4],[2.5]}. The expansion waves cause a gradual decrease of the core radius, whereas the vortex shock is typified by an abrupt increase in core radius as it propagates along the vortex. These pressure waves are considered to be an important source of sound.

As the cut vortex moves in chordwise direction misalignments in both chordwise and spanwise direction arise. Normally the flow velocities at the upper side of the wing are higher than at the lower side. This means that the vortex part that moves along the upper side is moving more quickly downstream than the vortex on the lower side, especially in the case of high angles of attack. This introduces a chordwise misalignment. The spanwise misalignment is due to two mechanisms; the image vortex effect and the gradient in the spanwise wing circulation. The image of the vortex induces an opposite movement of the upper and lower halves of the tip vortices. This phenomenon is illustrated in Figure 2.7a and b. If the direction of rotation of the propeller is clockwise when viewed from downstream then the part of the tip vortex that hits the wing at the side where the propeller blades move in upward direction (rotation-up) rotates in the direction as indicated in Figure 2.7a. It can be shown (Figure 2.8) that the direction of rotation of the component in chordwise direction of the tip vortex vector is always counterclockwise when viewed from downstream. This will also be the case for the image vortices. Because of their relative positions the image vortices induce velocities in opposite spanwise directions, see Figure 2.7b. This means that the two halves of the vortex 'ring' are sheared with respect to each other (Figure 2.7a). At low angles of attack the amount of shearing is about the same on both sides of the wing. But at higher angles of attack the angle between the normal to the wing and the tipvortex vector increases in magnitude on the rotation-up side and decreases on the rotation-down side (Figure 2.8). Therefore the component in the chordwise direction of the rotation-up side is stronger than

that on the rotation-down side resulting in more shearing of the vortex at the rotation-up side. The second mechanism of spanwise tip vortex motion is due to changes in the spanwise wing lift or circulation due to the slipstream. Due to the induction of upwash and downwash in the propeller slipstream tube (Figure 2.3) the circulation in spanwise direction will have large gradients in this region. Therefore the vortices that spring off the wing in this region will be considerably stronger than in other regions (except for the wingtip). These vortices again induce opposite spanwise velocity components at the upper and lower wing sides and, hence, opposite propeller tip vortex movement. Both of the described mechanisms act simultaneously, they can re-enforce or counteract each other depending on magnitudes and direction.

When the sheared tip vortex leaves the wing trailing edge a reconnection process takes place between the separated vortex filament parts. This phenomenon is not yet fully understood and is a subject for further study. Vorticity shed from the wing trailing edge, due to the unsteady loading experienced by the wing, is thought to participate in joining the vortex filaments^[2,3]. In this process viscous effects play an important role.

The factors described above seriously complicate the modelling of the propeller wake. Especially in high loading cases and low forward speed the helical shape of the wake is distorted. Even the more sophisticated classical methods like the Theodorsen method and panel methods still use the helical shape of the slipstream. Therefore only field methods which calculate the actual structure of the distributed vorticity field behind the propeller will be able to model the distorted wake. These methods will be dealt with in Chapters 3 and 4.

2.1.4 Viscous effects in the boundary layer on the blade

As on every wetted surface of an airplane, a boundary layer develops on the surface of the propeller blades. In the boundary layer the friction forces have a considerable influence. In a boundary layer the velocity varies from zero at the surface to the value of the velocity in the inviscid outer flow region. The fluid particles close to the blade surface are moving along with the blade motion and experience the same centrifugal acceleration as the blade itself. The centrifugal acceleration is proportional to the distance to the hub and accelerates the particles away from it. This is why in propeller boundary layer flows the velocity can have a considerable radial velocity component. Significant radial flow exists in separated flow regions and in laminar separation bubbles^{[2,6],[2,8]}. This results in large differences in the lift and drag coefficients computed using 2D or 3D theory.

The centrifugal force is not the only additional force in the propeller boundary layer. There is also the Coriolis force which acts on the particles moving in radial direction. This force accelerates the flow particles in downstream direction and stabilizes the boundary layer. Its effect can be compared with that of a favorable pressure gradient.

The forces that are mentioned influence the behaviour of the boundary layer. Because of the chordwise acceleration the separation of the boundary layer is usually postponed up to higher angles of attack of the propeller blade. The acceleration leads to a smaller displacement thickness of the boundary layer and consequently to less decambering of the section profiles. The boundary layer at the root sections is removed by the radial boundary layer flow that will

postpone the separation even further. This is why the maximum attainable lift coefficients become larger when moving from the tip to the root of the blade. In McCroskey^[2.7] it is argued that the stall delay effect is present up to 70% of the propeller radius. Some empirical correction methods can be found in Corrigan^[2.9]. Also the displacement effect can be mentioned of the boundary layer on the nacelle on the flow over the propeller blade sections near the hub. This effect results in higher local Mach numbers of the onset flow of these sections.

A very important phenomenon is the formation of a compact, well-ordered vortex along the leading-edge of thin propeller blades with substantial sweep at high loading conditions. This phenomenon is similar to the leading-edge vortex on delta wings at high angle of attack. This leading-edge vortex emerges because of flow separation at the leading-edge and can lead to a substantial lower pressure on the suction side of the blade compared to the stalled low-sweep blade where the vortex does not form. Therefore the highly swept blade can be used at higher blade pitch angles and thus at higher blade loading.

The 3D boundary layer flow is very complicated and difficult to calculate accurately. Therefore in the classical propeller methods the viscous effects on the blades are often ignored or simplified greatly (by using experimental 2D data). This means that these methods are not very reliable for propeller operating conditions at which the boundary layer flow is substantially affecting the characteristics of the flow. These cases are, as mentioned earlier, the high loading case in which the propeller blades are close to stall and cases in which the propeller onset flow is at high angle with respect to the propeller axis.

2.2 Review of classical propeller modelling methods

In the past, great effort has been put into understanding the characteristic flow phenomena of propeller slipstreams and to model these flows as accurate as possible. The purpose of which was to contribute to the development and integration of improved propulsion systems in aircraft and naval vessels. In the next section a review is given of the most important classical propeller models and their specific characteristics. The object is not to go in too much detail but rather to provide a background to the more recent Euler methods for propeller flow modelling that will be described in Chapter 4 and 5. In the present report the many potential flow methods that also can be used to model propeller flows are not discussed. In Heyma^[2.10] a survey of these methods can be found.

The development of the propeller theories followed two independent lines of thought. These resulted in the momentum theories and the blade-element theories, respectively. In a momentum theory attention is directed mainly to the motion of the fluid and the forces acting on the propeller are determined as the cause of this motion. In that way the exact shape of the propeller is not relevant. Only the forces that the propeller imparts on the flow are important. In contrast to that, the blade-element theories and their derivatives, the vortex theories, use the aerodynamic characteristics of the propeller blade sections to determine the aerodynamic forces.

2.2.1 Momentum theories

The earliest theories of the action of screw propellers date from the pioneering work of Rankine and Froude. Their initial application has been in marine propulsion systems. In the momentum theory the propeller is modelled as an infinitely thin actuator disc which exerts a distributed force on the flow field. Two versions of the momentum theory exist; the axial momentum theory and the general momentum theory. Both theories will be described briefly. Relevant information can be found in Glauert^[2,11].

The axial momentum theory of Rankine and Froude

In the axial momentum theory the flow is considered incompressible, inviscid and uniform in each axial section of the slipstream tube. The thrust generated by the propeller is considered uniformly distributed over the propeller disc. At the disc a jump in static and total pressure arises due to the propeller thrust. The axial velocity is continuous.

The thrust of a propeller can be calculated by subtracting the momentum of the flow entering and leaving a cylindrical domain (Figure 2.9) or by integrating the pressure difference across the disc:

$$T = \int_s \Delta p \, dS = S_1 \rho V_1 (V_1 - V_0) \quad (2.3)$$

Furthermore the propeller power can be calculated by subtracting the kinetic energy of the flow entering and leaving the domain:

$$P = \frac{1}{2} S_1 \rho V_1 (V_1^2 - V_0^2) \quad (2.4)$$

It is also possible to calculate the propulsion efficiency:

$$\eta = \frac{V_0 T}{P} = \frac{1}{1 + \left(\frac{V_1 - V_0}{2V_0}\right)} \quad (2.5)$$

Here, the efficiency is the maximum theoretically obtainable efficiency that can be achieved using a specific propeller because induced tangential and radial flow velocities as well as viscous effects are neglected. The lower the velocity difference across the propeller disc the higher the efficiency. The efficiency reaches 100% if the velocity increment approaches zero.

If the geometry of the slipstream tube is known, also the velocity and pressure in the slipstream can be obtained. This is done by using mass conservation and by applying the Bernoulli equation. It can be shown that the axial velocity at the propeller disc is the mean value of the velocities at the upstream and downstream boundaries of the domain:

$$U_{\text{disc}} = \frac{1}{2}(V_1 + V_0) \quad (2.6)$$

The general momentum theory of Betz

In the real propeller slipstream a rotational motion is present due to the tangential force exerted by the propeller on the air. In the general momentum theory the rotational character of the slipstream is taken into account by introducing an angular velocity jump with a constant angular momentum along the radius of the propeller disc. The rotational velocity (ω) in the propeller slipstream is directly related to the angular velocity (Ω) of the propeller and a tangential interference factor $a' = V_t/V$, in which V_t is the tangential component of the velocity V in the propeller slipstream. Application of the Bernoulli relation results in an expression for the pressure increase over the propeller disc:

$$p' = \rho \left(\Omega - \frac{1}{2} \omega \right) \omega r^2 \quad (2.7)$$

Again the thrust can be calculated by integration of p' over the propeller disc but also by using a momentum balance. Because of the rotational motion in the slipstream the pressure is not uniform at downstream infinity but varies radially to balance the centrifugal force:

$$\frac{dp_1}{dr_1} = \rho \omega_1^2 r_1 \quad (2.8)$$

The thrust follows with:

$$T = \int_s p' dS = \int_s [\rho V_1 (V_1 - V_0) - (p_0 - p_1)] dS \quad (2.9)$$

The torque that is acting on the propeller can be calculated by summation of the angular momentum imparted in unit time:

$$Q = \int_s \rho u \omega r^2 dS \quad (2.10)$$

The propeller power is calculated in the same manner as in the axial momentum theory but now the kinetic energy of the rotational motion is included. This leads to a lower and more realistic value of the propulsion efficiency. The best efficiency in a propeller design is obtained by optimally distributing the thrust in radial direction. In this case the efficiency of all blade elements is constant ^[2.11].

In general it can be stated that momentum methods provide a simple relation between the velocities in the propeller wake and the thrust and torque of the propeller. However, because of the many assumptions made and because the actual shape of the propeller is not considered the momentum methods are not very suitable to calculate accurate jump conditions for the more advanced mathematical models that can be used to calculate the flow around propellers.

2.2.2 Blade-element theories

The first simple blade-element theory was proposed by Froude and was further developed by S. Drzewiecki and W.F. Lanchester^[2.11]. In contrast to the momentum theories, the blade-element theory is concerned with the actual aerodynamic shape of the propeller. The basis of the analysis is that the propeller blade is divided into a large number of elements along the propeller bladespan and that each of these elements is regarded as a 2-D airfoil section. The theory requires that the aerodynamic properties (lift and drag coefficients) of the airfoil sections are known. Viscous effects, like propeller stall and compressibility effects can thus be incorporated (quasi-3D). Each blade-element has an angle of attack determined by the tangential and axial components of the local velocity. The induced velocities due to the surrounding environment are not included. Total lift (thrust) and drag forces of the propeller are calculated by integration of the section properties.

The method lacks accuracy because of the assumptions made in the theory. In reality the flow around the blades is not two dimensional. The finiteness of the propeller blade influences the lift and drag distribution so that the 3-D and the 2-D coefficients do not match. Furthermore the velocity induced by the vorticity in the wake is neglected. This results in errors in the angle of attack of the onset flow of the blades and consequently in errors in lift and drag forces and in the predicted propeller performance. Also interference effects between successive blade-elements are neglected. Aerodynamic characteristics are not corrected for these effects.

The simple blade-element theory forms the basis for the later developed strip analysis theories or vortex theories. In these theories corrections are introduced for the induced velocity by the wake and the influence of the surroundings. In the next section the basics of these vortex theories are described.

2.2.3 Vortex theories

In propeller vortex theories the influence of the vorticity in the slipstream on the blade is included. This is achieved by prescribing the shape of the wake and calculating its induced velocity at the propeller disc. In the next section three methods are described; the theory of Betz, Glauert and Prandtl, the theory of Goldstein and the theory of Theodorsen. In all three theories the wake model that is used is based on a blade loading distribution for minimum induced loss. The theories differ in the detail in which the wake is described and in their complexity.

The theory of Betz, Glauert and Prandtl

In the vortex theory developed by Betz, Glauert and Prandtl the wake of the propeller is treated as a rigid cylinder. The propeller is assumed to have a infinitely large number of blades and the circulation along the bladespan is assumed to be constant. This implies that the vorticity springing from the blade trailing edge is concentrated at the edge of the propeller disc. This vorticity is transported downstream without contraction of the slipstream. Thus, the combined vorticity of the infinite number of blades can be represented as a rigid cylinder

surface carrying a spiraling vortex distribution, see Figure 2.10. At the axis of symmetry a straight root or hub vortex is present which can be considered the combined return leg of all vortex lines on the propeller disc.

This way of treating the propeller wake has some consequences. As in the momentum methods all time-dependent characteristics of the slipstream are lost. Due to the assumption of an infinitely large number of blades there are no discrete vortex sheets that interact with the flow outside the slipstream tube. Therefore the radial velocity component will not be present in the slipstream (in case of axi-symmetrical onset flow). It should also be mentioned that neglecting the contraction of the slipstream is only valid in the case of lightly loaded propeller blades.

Due to the simple geometry of the wake, the induced axial and azimuthal components of the velocity and the circulation at each radial position in the slipstream at downstream infinity can easily be calculated^[2.11]. As in the momentum theories the induced axial component of the velocity at the propeller disc is half the value of the axial velocity at downstream infinity. This means that the induced velocities at the disc can be determined if the velocity distribution in the wake is known. The operating condition of the propeller blade sections can be determined and the section characteristics can be calculated by application of the blade-element theory. Again integration along the blade radius and summation of the contributions of all blades will lead to the total thrust, the total torque and the propulsion efficiency.

The vortex theory can also be used to design propeller blades that lead to a minimum loss of energy or to the highest efficiency for a given thrust. It can be shown that the condition of minimal energy loss is related to a certain optimal circulation distribution in the far wake. This distribution is identical to the circulation distribution around the propeller blades. The circulation around each blade section can be obtained by dividing the total circulation at a certain radial position by the number of blades. The resulting lift and drag due to the blade section circulation can be calculated by using Joukowski's law. Integration of the blade section contributions along the blade will lead to the total thrust, torque and efficiency of the propeller.

Two corrections can be found in literature to improve the results of the above vortex theory. The first one is a correction for the profile drag (if this is not already included in the section drag coefficient). The introduction of profile drag, assuming the same distribution of circulation along the blade, will reduce the thrust and increase the torque of the propeller and thus will lead to a lower propulsion efficiency. Profile drag will also lead to a different optimal distribution of the circulation around a blade. The second correction is for the finiteness of the number of blades and was proposed by Prandtl. As described earlier in the real propeller flow the vortex sheets can be assumed to be rigid surfaces that move backwards at a constant speed. Near the edge of the vortex sheets the air will tend to flow around the edges of the sheets resulting in considerable radial velocity components. These radial velocities cause a decrease in circulation in the tip region of the propeller blades. To account for this effect a comparison is made with an equivalent flow around the edges of a number of flat plates moving with the same speed as the vortex sheets. A tip loss factor can be deduced that adjusts the circulation distribution in the tip-region. For propeller analysis

calculations an effective radius is defined that replaces the actual radius in the calculations.

The theory of Goldstein

In contrast to the vortex method of Betz, the theory of Goldstein^[2.12] takes account of the periodic nature of the slipstream. Each blade is modelled by a single bound vortex with a varying circulation distribution in radial direction. Because of this, a vortex sheet of varying strength in radial direction is springing from the blade trailing edge. As in the vortex theory of Betz the propeller loading is considered to be light. In that case the vortex sheets will have a helical shape with a constant slope which follows from the forward velocity and the rotational velocity of the propeller. In the theory no contraction of the slipstream tube or roll-up of the vortex sheets is considered.

The 3D surfaces of the vortex sheets induce velocities in the slipstream. The equation of the vortex surface of a single blade far behind the propeller is given by:

$$\theta - \frac{\omega z}{V_{\infty}} = 0 \quad \text{or} \quad \pi \quad \text{for} \quad r < R \quad (2.11)$$

r , θ and z are the cylindrical polar coordinates with the helix axis as the reference axis and ω is the rotational velocity of the wake. V_{∞} is the unperturbed onset flow velocity of the propeller.

Goldstein introduced a velocity potential function which he calculated at far downstream by solving the Laplace equation. This velocity potential has to satisfy certain boundary conditions in the cross-section far downstream. By introducing a curvilinear coordinate system he was able to reduce the three-dimensional flow problem to a two-dimensional problem. The solution for the potential is expressed in a semi-infinite series of modified Bessel functions.

Goldstein was able to construct the solution for the potential only in case of small values of the advance ratio (V/nD). The circulation around an arbitrary blade section is assumed to be identical to the jump in the velocity potential at the corresponding point in radial direction of the vortex sheet. Thus the circulation around the blade is determined directly by the velocity potential.

In the Goldstein theory the circulation around the blade is expressed in terms of a non-dimensional K-function defined as:

$$K = \frac{B\omega\Gamma(r/R)}{2\pi w V_{\infty}} \quad (2.12)$$

Here Γ is the circulation as a function of (r/R) and B is the number of blades. Different K-functions can be calculated for propellers with different number of blades. The K-function forms a correction on the induced velocity calculated for a propeller with an infinite number of blades (like the Prandtl tip loss factor). The value of K tends to unity as the number of blades tends to infinity and the propeller becomes an actuator disc. The value of K tends to

zero at the blade tip for any finite number of blades, where the blade loses its circulation. The K-functions are obtained from tables and an additional interpolation procedure or by calculation of the Bessel functions. Also finite-difference and finite-element methods for solving the potential-flow problem can be found in Wentzel^[2,13].

If the flow properties at a downstream station are known (for example from experiments) then the circulation distribution along the propeller blade can be calculated. Using Joukowski's law the thrust loading, torque loading and the efficiency can be related to the K-function. The total propeller thrust, torque and efficiency can be calculated by integration along the blade radius. It should be mentioned that the Goldstein theory is not intended to give a detailed description of the propeller slipstream. The solution of the potential problem is only valid in the far field.

At propeller efficiencies well below unity the Goldstein vortex theory can provide unreliable results. This is because the theory is based on a circulation distribution for minimum induced loss. This optimal distribution is of course not always present. Also for blades with low advance ratios the theory does not account for 3-D effects and unreliable results can be expected.

Theodorsen's theory

Theodorsen's theory^[2,15] is largely based on Goldstein's vortex theory. Theodorsen showed that Betz's theorem of the optimum distribution of circulation applies equally well to heavily loaded propellers if reference is made to the shape of the helix infinitely far behind the propeller. The radial distribution of the circulation in the far field wake behind a heavily loaded propeller is the same as that obtained by Goldstein for the propeller at light loading, if the results are compared for the same value of the helix angle. In this theory the heavy loading case is equivalent to an infinite number of lightly loaded propellers placed serially behind each other. Each lightly loaded propeller has an optimum circulation distribution.

Theodorsen defines the following equation for the vortex surface:

$$\theta = \frac{\omega z}{V_{\infty} + w} = 0 \text{ or } \pi \quad 0 \leq r \leq R \quad (2.13)$$

This formula contains w , the axial component of the velocity of the screw surface in axial direction, which cannot be neglected anymore with regard to the velocity at infinity (as in Goldstein's theory). The velocity w can be viewed as an independent parameter upon which all other quantities depend. The proper value of w must be obtained by iteration.

Furthermore Theodorsen defines a circulation function K (like Goldstein), a mass coefficient κ and an axial tip loss factor ϵ . Only the K and κ functions contain the unknown circulation. ϵ is directly related to κ . Instead of calculating the K and κ functions Theodorsen used experiments. An analogy can be made between a potential flow and the electrical potential in a waterbasin containing a physical model of the helical vortex sheets. The resulting voltage distribution is related to the velocity potential in the propeller slipstream. The K-functions can

thus be obtained physically. The mass coefficient κ can be compared physically to the blocking effect of the helical surface. It is obtained experimentally by measuring the change in resistance caused by the helical surface when it is inserted in the waterbasin. Theodorsen obtained loading functions for a variety of propeller types and working conditions. Some examples are; highly loaded propellers with high advance ratios, propellers with large number of blades, counter-rotating propellers and propellers with guide vanes.

Calculation of the propeller characteristics is done by means of an iteration process. The loading distribution on the blade and the functions K , κ and ϵ all depend on the unknown velocity w . An initial guess is made for w which together with the proper aerodynamic coefficients determine an initial loading distribution on the propeller blade. The loading distribution on the blade is linked to the far-field conditions via the K , κ and ϵ functions. These are also related to w , so a new approximation for w can be obtained. This process converges to the proper w and loading distribution. Thrust, torque and propulsion efficiency are all related to the K , κ and ϵ functions and can be obtained easily.

2.3 Pros and cons of the different theories

When comparing the different propeller models it is obvious that even the most sophisticated and complete model (Theodorsen) only gives an approximation of the real flow field of the propeller and its slipstream. In the next section the limitations of the different theories are summarized as well as their relative advantages. It must be realized that the described theories have different application areas. It is not possible to treat the entire propeller flow field with one universal theory. In practice the different theories are combined into a single propeller analysis method.

None of the described propeller theories are suited for treating propellers at an angle of attack. This is particularly the case for vortex theories in which the shape of the wake is prescribed. The slipstream of a propeller at an angle of attack is highly time-dependent. Thus the conditions in the propeller plane are not merely depending on the (azimuthal) position of the blades but also on the continuously varying strength of the vorticity in the wake. The loading distribution on the propeller blade is therefore not like the optimum distribution according to Betz. Also the considerable radial flow on the blades prohibits the use of 2D aerodynamic section data. One case is found however in Eshelby^[2,14] where the blade-element theory is used to calculate unsteady forces and moments under the restriction of small angles of attack.

Momentum theories

Momentum theories are easy to implement because of their simple formulation. However, this is at the expense of some serious disadvantages which may lead to very unreliable results.

Momentum theories treat the propeller as an actuator disc. They can only be used if conditions in the propeller plane (static and total pressures, induced velocities and swirl angles) are known. Therefore these methods need experimental propeller data or the results

of a propeller theory which calculates the conditions in the plane of the propeller.

Momentum theories give only a time-averaged approximation of the real, time-dependent propeller slipstream while ignoring compressibility and viscous effects. The general momentum theory gives more realistic results than the axial momentum theory because it includes tangential velocity components as well as a varying disc loading. However, a detailed representation of the propeller slipstream with shed vorticity, wake roll-up and wake induced radial flow is not possible with these theories. Momentum theories also give wrong results in the far field wake because velocities go to a final value other than the free stream conditions.

Blade-element theories

Simple blade-element theories use the aerodynamic shape of the propeller blades. However, the problem is that 2D section data is used for the propeller blade sections. The aspect ratio effect therefore is neglected. The 2D section data include effects of viscosity and compressibility, but 3D effects are neglected. Also induced velocities that influence the effective angle of attack of the blade are ignored. A wake model is therefore needed that accounts for these effects. Without a proper wake model the blade-element theory will not be very accurate.

Blade-element theories only treat the flow around the propeller blades. No information about the propeller slipstream can be obtained by using this theory.

Vortex theories

In the theories of Prandtl, Goldstein and Theodorsen the shape of the wake is prescribed. This shape is based on a loading distribution for minimum induced loss. In that case deformation, roll-up of the vortex sheets are considered as second-order effects at the propeller plane and can be ignored. Immediately it can be understood that the wake model is only valid if the propeller blade loading is not very much different from the optimal loading condition. In flight conditions such as take-off and landing this is not the case and even the most sophisticated analytical theory of Theodorsen will fail. Furthermore the shape of the vortex sheets at infinity is also influenced by the presence of bodies in the slipstream. These bodies can distort the slipstream considerably (shearing) so that the idealized shape is not present.

The vortex models all ignore the radial flow on the blades. This radial flow can considerably change the aerodynamic coefficients of the blade sections. Radial flow develops at the blade tip due to the contraction of the slipstream (especially at high disc loading), due to possibly curved leading and trailing edges of the blade, due to centrifugal forces especially in regions of separation or at the blade root due to the presence of the nacelle and spinner. Besides this coriolis forces may seriously affect the boundary layer behaviour and therefore influence the aerodynamic coefficients.

In the Prandtl and Goldstein theories only light loading of the propeller blade is considered. They also ignore the contraction of the slipstream. The theory of Theodorsen also treats the high loading case including the contraction effect. However, it must be mentioned that even

the Theodorsen theory will fail in cases such as the modern propfan propellers. On these very thin propfan blades flow separation effects lead to rolled-up vortex sheets along the leading-edge. These effects cannot be modelled by the Theodorsen theory. Of course also the considerable radial flow over the blades due to the extremely curved shape of the propfan blade will invalidate the use of these vortex models.

Goldstein's theory is in principle more accurate than the Prandtl theory. Because of its accuracy, it is often used for performance calculations and propeller design. However, because of its more complicated wake model its application takes a considerable computing effort compared to the Prandtl theory. This is also the case for the Theodorsen theory. Numerical methods are used in these theories that call for the use of computers.

The models of Prandtl, Goldstein and Theodorsen are primarily used for the calculation of the condition at the propeller plane. From far wake conditions the discontinuity in velocity potential is calculated, which is a measure for the circulation around the corresponding blade section at the propeller plane and the velocities that are induced by the vortex system. The calculated velocity potential is only valid in the wake far downstream. Therefore, only far-wake field information can be obtained with the described theories.

Theodorsen^[2.15] performed calculations to determine the static pressure in the propeller slipstream but this led to disappointing results. A better model can be found in Schouten^[2.16]. If information is needed about the wake in the neighbourhood of the propeller these models cannot be used. A combination of these models and a momentum theory is then required.

2.4 Propeller jump conditions for Euler methods

In Chapter 5 of this report an actuator disc representation of the propeller will be described in combination with an advanced free-wake analysis method (Euler method). In this method the exact time-averaged shape of the wake is calculated. An auxiliary propeller model must be used to provide the flow jump conditions at the propeller disc because the propeller shape is not included in this model.

In principle the solution of a method based on the Euler equations will automatically include the time-averaged induced velocities in the propeller plane due to the distributed vorticity which is present in a propeller slipstream. An iterative process can be used in which the conditions in the propeller plane are calculated using the simple blade-element theory without a separate wake model. The jump conditions that can be obtained from it are imposed as boundary conditions for the Euler method. This method then calculates a new, improved, wake which induces different velocities at the propeller plane. If this process converges properly the correct loading on the propeller is obtained with the correct shape of the wake. It must be remarked that the used blade-element model must be corrected for 3D effects (aspect ratio) and for interference effects between the blades (cascade effect), because these interference effects cannot be calculated by the Euler method.

The selection of the propeller model depends on the information which is available about the propeller. If for instance the forces on the propeller blades are known from measurements, the required jump conditions can be obtained by using the general momentum theory. An alternative method is described in Chapter 5 in which source terms are added in the set of flow equations. If this information is not available then the most accurate model is of course preferred (Theodorsen).

3 Introduction into Euler methods

This chapter is intended to give a brief introduction into the basics of Euler methods as far as is needed for understanding their application to the calculation of propeller flows. The Euler equations are compared to other flow equations and their mutual relations are explained. The general solution procedure in Euler methods is described as is the way in which the initial and boundary conditions are treated. The propeller slipstream flow around an aircraft is described as an initial-boundary-value problem that can be treated successfully with Euler methods. It is explained that the power of Euler methods in propeller flows lies in the fact that their solution includes the propeller wake. In that case the need for a separate propeller wake model is eliminated.

3.1 Hierarchy of flow equations

The most general set of equations describing airflows is the set Navier-Stokes equations. The time-dependent Navier-Stokes equations describe the conservation of mass, momentum and energy for general flows. The basic forces acting in these flows are pressure forces and friction forces. Temperature effects like heat dissipation resulting from friction and heat transfer are also modelled in these equations. For the present study air may be considered a so-called Newtonian fluid. In Newtonian fluids the viscous stresses are directly proportional to the rate of deformation of the fluid particles while the heat flux vector is given by Fourier's law that is proportional to the gradient of the temperature field. Solution of the system of Navier-Stokes equations, supplemented by thermodynamic relations, is a very difficult task because of the complexity of the equations (e.g. turbulence). Fortunately it can be observed that not all of the flow phenomena are equally important in all parts of the flow field. In these cases assumptions can be made to simplify the problem. All other types of flow equations can be derived from the Navier Stokes equations by using such assumptions. The more assumptions are made the more restricted is the validity domain of the resulting flow model.

If the friction forces and the heat dissipation are neglected the next hierarchical level of flow equations is obtained; the Euler equations. These equations describe inviscid, compressible, rotational flows. In the next section they will be described in more detail.

If the vorticity of the flow is neglected, the velocity can be expressed as the gradient of a velocity potential while assuming isentropic flow. The mass conservation equation can then be written in terms of the velocity potential, the so-called full-potential equation. The momentum equation reduces to Bernoulli's relation from which for a known velocity field the pressure and density can be obtained. For irrotational, isentropic, flows the energy conservation equation is satisfied automatically and does not need to be considered explicitly. Therefore only the full-potential equation remains. If the full potential equation is linearized the so-called Prandtl-Glauert equation can be deduced. This equation describes compressible

flow only in a linearized fashion. Finally, if the compressibility of the flow is neglected the Laplace equation is the governing equation for the velocity potential.

3.2 Introduction of the Euler equations

As described in Section 3.1 the equations describing time-dependent, adiabatic, compressible flow of an inviscid, non-heat-conducting fluid are called the Euler equations. In integral conservation form these conservation equations using vector notation, take the following form.

Conservation of mass:

$$\frac{\partial}{\partial t} \iiint_V \rho dV + \iint_{\partial V} \rho \vec{u} \cdot \vec{n} dS = 0 \quad (3.1)$$

Newton's second law:

$$\frac{\partial}{\partial t} \iiint_V \rho \vec{u} dV + \iint_{\partial V} \rho \vec{u} (\vec{u} \cdot \vec{n}) dS = - \iint_{\partial V} p \vec{n} dS \quad (3.2)$$

Conservation of energy:

$$\frac{\partial}{\partial t} \iiint_V \rho E dV + \iint_{\partial V} \rho E (\vec{u} \cdot \vec{n}) dS = - \iint_{\partial V} p \vec{u} \cdot \vec{n} dS \quad (3.3)$$

Here V is the control volume with its surface S and with \vec{n} the local normal vector on S . The total energy E , for a calorically perfect gas is defined by:

$$E = \frac{p}{(\gamma-1)\rho} + \frac{1}{2} \vec{U}^2 \quad (3.4)$$

in which the velocity vector \vec{U} :

$$\vec{U} = (u, v, w)^T \quad (3.5)$$

Here u , v and w are the velocity components in respectively x , y and z directions. ρ is the density and p is the static pressure.

The Euler equations constitute a system of first-order non-linear partial-differential equations. The non-linearity has serious consequences for the solution of the Euler equations. In panel methods (linearized potential flow methods) the 3D flow equation is reduced to a surface integral equation using Green's theorem. Because of the non-linearity of the Euler equations,

this reduction is no longer possible. Discretization of the Euler equations in 3D space (in case of a 3D problem) is thus required.

The general approach to the numerical solution of the Euler equations consist of two major steps.

- Spatial discretization of the flow equations and the boundary conditions of the continuum-model formulation of the problem.
- Solving the resulting system of ordinary differential equations.

In the next section the general solution procedure of the Euler equations will be described.

3.3 Solution procedure in Euler methods

In this section the basic procedure for solving the system of Euler equations is described. Some discretization approaches are mentioned and the concept of numerical viscosity is introduced. The method for obtaining the solution for the resulting system of discretized equations is also described. Use was made of Boerstoele^[3.1].

3.3.1 Discretization of the system of equations

Usually the system of Euler equations as described in Section 3.1 is discretized by a finite-volume discretization. The Euler equations in integral form as described in Section 3.1 can be used locally for each finite volume (cell). The system can be written as:

$$\frac{\partial}{\partial t} \iiint_{\Omega} \bar{q} d\Omega + \iint_{\partial\Omega} \bar{F} \bar{n} dS = 0 \quad (3.6)$$

with \bar{q} the vector of conserved quantities:

$$\bar{q} = (\rho, \rho U, \rho V, \rho W, \rho E)^T \quad (3.7)$$

and \bar{F} the flux tensor:

$$\bar{F} = \begin{pmatrix} \rho U \\ \rho U^2 + p \\ \rho UV \\ \rho UW \\ \rho UH \end{pmatrix} \bar{i} + \begin{pmatrix} \rho V \\ \rho UV \\ \rho V^2 + p \\ \rho VW \\ \rho VH \end{pmatrix} \bar{j} + \begin{pmatrix} \rho W \\ \rho UW \\ \rho VW \\ \rho W^2 + p \\ \rho WH \end{pmatrix} \bar{k} \quad (3.8)$$

with the total enthalpy H defined by:

$$H = E + \frac{P}{\rho} \quad (3.9)$$

These equations can be discretized by so-called semi-discretization. This means that first the equations are discretized in space. The equations are then transformed into a system of ordinary differential equations with time as the independent variable:

$$\frac{d}{dt}(h_{i,j,k} \bar{q}_{i,j,k}) + \bar{Q}_{i,j,k} = 0 \quad (3.10)$$

Here $h_{i,j,k}$ is the volume of cell i,j,k and $Q_{i,j,k}$ is the net flux out of the cell given by:

$$\bar{Q}_{i,j,k} = (\bar{F} \cdot \bar{S})_{i+1/2,j,k} - (\bar{F} \cdot \bar{S})_{i-1/2,j,k} + (\bar{F} \cdot \bar{S})_{i,j+1/2,k} - (\bar{F} \cdot \bar{S})_{i,j-1/2,k} + (\bar{F} \cdot \bar{S})_{i,j,k+1/2} - (\bar{F} \cdot \bar{S})_{i,j,k-1/2} \quad (3.11)$$

S is the surface of a cell face. This system of ordinary differential equations can be integrated in time using for example an explicit scheme such as a Runge-Kutta method. The spatial discretization is done by dividing the physical domain into a sufficiently large number of cells (grid generation). The distribution of cells should be such that in areas where the flow has large gradients the grid is locally refined (Figure 3.1). The cells should be solid boundary conforming (follow the surface) so that boundary conditions can be implemented easily. The system of Euler equations in integral conservation form has to be satisfied for each cell. Therefore, the flux tensor must be calculated at the cell faces. This can be done in a number of ways.

The easiest and most widespread method at the moment is the central-differencing method used by Jameson^[3,2]. In this scheme the flux terms at the cell-face midpoints are taken as the average of the fluxes evaluated at the adjacent cell centres. For the 2D case this central differencing scheme is illustrated in Figure 3.2.

Another method for calculating the flux is by using the so-called approximate solution of the one-dimensional Riemann problem. A detailed description of this method is beyond the scope of this study. The reader is referred to literature on this subject^{[3,3],[3,4]}. The essence of the method lies in utilizing the hyperbolic nature of the Euler equations and using information obtained along the local characteristics to calculate the fluxes. This is done by using so-called 'upwind' differences, see Figures 3.3 and 3.4, instead of central differences. Later on some specific qualities of these differences are described. Characteristics of a hyperbolic system of differential equations running through a point in space determine the domain (dependence domain) that influences the flow conditions in that point through propagation of the perturbation waves. This is very similar to Mach lines in supersonic 2D flow.

3.3.2 The concept of numerical viscosity

A very important property of Euler methods is that distributed vorticity is included in the solution. When expressed in integral conservation form Euler methods allow solutions with vorticity concentrated in vortex sheets. This is of great value for the calculation of propeller slipstreams. Also shockwave type discontinuities with associated production of entropy and

vorticity are modelled in Euler methods. However, the vorticity due to flow separation is not included in the mathematical model and has to be modelled through Kutta-type conditions. The convection and stretching of vorticity in the propeller wake, is calculated as part of the solution and a wake model is not required. Responsible for the generation of vorticity at sharp edges are numerical dissipation terms that are added to the discretized system of equations. There are two ways to add these terms:

- 1) They can be added implicitly as in 'upwind' schemes, see Figures 3.3 and 3.4. Using these schemes automatically incorporates damping terms for the truncation error that arise because of the discretization. Because the system of equations is hyperbolic the direction in which these differences must be taken depends on the characteristics of the equations. For explicit schemes the domain of dependence of the numerical scheme should contain the domain of dependence of the differential equation (CFL condition for numerical stability). The magnitude of the artificial dissipation is controlled by the properties of the grid.
- 2) They are added explicitly to the discretized equations and the user can control their magnitude through input parameters. This is required when a 'conventional' central differencing scheme (Figure 3.2) is used. This scheme does not automatically incorporate these additional terms.

Numerical dissipation or numerical viscosity acts as a means of smoothing the solution and takes care of the elimination of non-physical solutions in case of shockwave discontinuities. Because the natural dissipation is not present in the Euler equations there is no mechanism that prevents expansion shocks in which the entropy drops rather than rises as prescribed by the 2nd law of thermodynamics. Without correction these non-physical solutions of the Euler equations can arise. The artificial dissipation terms add an entropy condition to the system.

3.3.3 Solution of the discretized system

For the solution of the system of equations it must be recalled that the flow that is treated might be time-dependent. As will be described in later chapters the flow in propeller slipstreams can be treated time-averaged or time-dependent. In the case of time-averaged flow the solution of the system of ordinary differential equation that results after spatial discretization of the Euler equations can be solved by integration in time until a steady solution is obtained. Integration methods like the Runge-Kutta scheme can be used for this. Acceleration methods like local time stepping (optimizing the local time stepsize with relation to stability criteria) can be used to speed up this iteration process. In the time-dependent case this acceleration is no longer possible because the solution must be calculated time-accurate.

3.4 Initial and boundary conditions for the flow problem

The system of Euler equations with initial and boundary conditions constitutes an initial/boundary value problem. The initial conditions are simply the initial values of the flow variables. Usually the undisturbed uniform flow is used or a quickly obtained solution on a coarse grid. At time $t=0$ the initial conditions are activated and the solution starts to develop. In the following a description is given of the boundary conditions that have to be imposed

on the solution of the Euler equations.

In general four types of boundary conditions can be mentioned. These boundary conditions are to be imposed at:

- Physical boundaries like the body surface;
- Far field boundaries of the computational domain;
- Boundaries at intakes or outlets of engines;
- Internal boundaries in the grid used for treating discontinuities in the solution such as an actuator disc

These types of boundary conditions will now be described briefly.

The physical boundaries of the flow domain are formed by physical objects like the solid surfaces of an aircraft. There is no mass flow across these boundaries resulting in a boundary condition for the normal component of the velocity:

$$\vec{U} \cdot \vec{n} = 0 \quad (3.12)$$

In some cases the influence of the boundary layer that is developing along the body surface is modelled by allowing a small normal velocity (transpiration boundary condition associated with the displacement thickness of the boundary layer).

At infinity the solution should approach the free-stream conditions, except possibly in the vortical wake at downstream infinity behind shock waves. Although a number of different approaches can be found in the literature the one using the theory of characteristics is described further.

Proper boundary conditions can be imposed by using the characteristic directions of the hyperbolic Euler equations. These directions prescribe the way in which wave-like disturbances propagate through the flow field. It is essential for the stability of the solution method that waves that leave the flow domain are not reflected back into the domain. In some methods this is done by splitting the incoming and outgoing fluxes at the boundary. Only the incoming fluxes are imposed as boundary conditions on the solution. Boundaries at intakes or outlets of air-breathing engines are treated in a similar way.

The last type of boundary conditions are the conditions for a discontinuity inside the flow domain. As will be described in Chapter 5 jump conditions can be imposed on the solution of the Euler method. Because the domain is divided in a large number of cells, the surface of a discontinuity can be thought of as being build up by the faces of the volume elements. For programming reasons the discontinuity is often aligned with a grid surface on which one of the coordinates is constant.

The boundary conditions described above have to be discretized along with the Euler equations. Depending on the discretization method, the boundary conditions can be accounted for at the cell faces that coincide with the boundaries. In some cases an interpolation might be necessary to fit the boundary conditions into the numerical scheme. In Chapters 4 and 5 the boundary conditions for propeller flows are treated in more detail.

3.5 The propeller slipstream as an initial-boundary-value problem.

As was discussed in Section 3.1 the Euler equations describe the class of inviscid, compressible, rotational flows. Especially the fact that distributed vorticity is included is of great value. In aircraft aerodynamics some flow types are highly dominated by vortical flow effects. Examples of these flows are:

- Flows with strong shock waves
- Fighter aircraft aerodynamics (low aspect ratio, high angle of attack)
- Flows involving the exhaust of turbofan engines
- Rotating systems like propellers and helicopter rotors

Therefore, Euler methods are better suited for simulating propeller slipstream flows than the methods discussed in Chapter 2.

In Chapter 2 an introduction has been given on the basic aerodynamics of propellers and propfan blades. It was explained that in principle the blades are rotating wings behind which a helical wake develops. In the real (time-dependent) flow these vortex sheets are convected downstream. The shape of this wake and the vorticity distribution in it is influenced by self-induction and by the presence of bodies (wing/nacelle) in the slipstream.

A description of the propeller slipstream problem in terms of an equivalent numerical initial/boundary value problem can be obtained as follows. The propeller flow problem constitutes the numerical approximation of the flow bounded by the surfaces of the aircraft together with the propeller blade surfaces. The blade boundary conditions are time-dependent. The self-influencing nature of the slipstream is simulated in Euler methods by the 'wave-like' propagation of the disturbances through the grid during execution of the iteration process. The shape and strength of the vortical slipstream can be automatically captured in the numerical solution if the computational grid is sufficiently refined in regions with concentrated vorticity. In the time-dependent case a self-adapting grid must be used that follows these regions during their journey through the flow field.

In the case of a time-averaged approach of the propeller slipstream the individual vortex wakes that are springing from the blade trailing edge are not captured in the solution. The vorticity is distributed continuously in the flow field. The benefit of this way of looking at the problem is that the flow can be treated as a steady flow. Here adapting grids might not be needed. The exact geometry of the propeller can be approximated by reducing the propeller to a discontinuity (the actuator disc) in the computational domain. In Chapter 5 this way of treating the propeller is described in more detail.

4 Unsteady propeller slipstream modelling

In some cases a detailed knowledge of the real, time-dependent behaviour of the flow field of a propeller can be crucial for the proper design of a propulsion system and its integration in the aircraft configuration. As an example can be mentioned the design of propfan propulsion systems. These propulsion systems, with their potential advantage in propulsion efficiency over turbofan engines, can only be designed properly if the designer is able to understand and predict the behaviour of the complicated flow field around the installed propfan. The unsteadiness of the flow caused by non-symmetric inflow of the propeller considerably affects the propfan performance and the noise levels. Propfans will have to operate at high subsonic speeds which will lead to regions in which supersonic flow exists over part of the propfan blades. Thus, the time-dependent motion of shockwaves and the associated wave drag are important subjects in the design of the propfan installation. Also the time-dependent loading of the propfan blades and the deflection of the blades under loading are problems which have to be understood before a suitable propfan configuration can be manufactured. The very thin blades of propfans are very flexible and catastrophic aeroelastic instabilities might arise.

As was described in Chapter 3, the flow field around a propeller and its slipstream can be simulated accurately by Euler methods. It was also argued that the propeller flow can be treated time-averaged or time-accurate. The time-averaged modelling of propellers is not suitable for propellers at angle of attack, although some examples are found in literature in which the propeller flow is modelled in a quasi-steady fashion by introducing inflow swirl ^[4.1]. In this chapter some recent time-accurate slipstream modelling techniques will be discussed. In these methods the aerodynamic shape of the propeller is included in the geometrical model of the configuration. This gives some problems regarding the proper application of boundary conditions on the propeller surfaces. A major difficulty arises in the generation of grids for bodies in relative motion. It is not possible to construct a single grid which wraps around both the propeller and the aircraft configuration. Therefore special grid construction techniques are used that will be described in this chapter.

In the literature on the subject of time-accurate propeller flow simulation with Euler methods two general ways of thought can be recognised. The first one is the quasi-steady modelling of the propeller flow field. In this method a reference system is used which is attached to the propeller and rotates along with it. If the propeller configuration is symmetrical with respect to the rotational axis, the time-dependent flow field can be viewed as a 'steady state' flow field in the rotating reference system. It is obvious that this modelling technique can only be used if the onset flow of the propeller configuration is axi-symmetric. The angle of attack of the onset flow therefore has to be zero. As will be remarked later on, this modelling technique allows a reduction of the required grid size because use can be made of the symmetry of the flowfield. The second modelling technique is the real time-dependent treatment of the propeller flow field. This technique can be used for any propeller configuration at any any operating condition including asymmetric flow conditions.

4.1 Quasi-steady modelling of propeller slipstreams

One of the first methods which could provide detailed solutions of propeller flow fields was an unsteady finite-difference Euler method (NASPROP) developed by Bober et al. [4.2],[4.3],[4.4] on the basis of Beam [4.5]. The method uses the quasi-steady modelling approach in which the flow field is considered to be steady with respect to a rotating reference system. It can only be used for axi-symmetrical configurations at symmetrical flow conditions.

4.1.1 Transformation of the Euler equations

In the NASPROP method the governing Euler equations in differential form are rewritten in cylindrical coordinates. A time-dependent mapping is applied and the Euler equations are transformed to a rotating, body-fitted curvilinear coordinate system. This is accomplished by the following transformation:

$$\begin{aligned}\xi &= \xi(t, z, r, \phi) \\ \eta &= \eta(t, z, r, \phi) \\ \zeta &= \zeta(t, z, r, \phi) \\ \tau &= t\end{aligned}\tag{4.1}$$

The system of PDE's then transforms to:

$$\frac{\partial Q}{\partial \tau} + \frac{\partial F}{\partial \xi} + \frac{\partial G}{\partial \eta} + \frac{\partial H}{\partial \zeta} + I = 0\tag{4.2}$$

where Q is the vector of the conserved quantities, F, G and H are flux vectors, and I is a source vector:

$$Q = J \begin{pmatrix} \rho \\ \rho u \\ \rho v \\ \rho w \\ E \end{pmatrix} \quad F = J \begin{pmatrix} \rho \bar{U} \\ \rho u \bar{U} + \xi_p p \\ \rho v \bar{U} + \xi_r p \\ \rho w \bar{U} + \xi_\phi \frac{p}{r} \\ \bar{U}(E+p) - \xi_p p \end{pmatrix}\tag{4.3}$$

$$G = J \begin{pmatrix} \rho V \\ \rho u \bar{V} + \eta_z p \\ \rho v \bar{V} + \eta_r p \\ \rho w \bar{V} + \eta_\phi \frac{p}{r} \\ \bar{V}(E+p) - \eta p \end{pmatrix} \quad H = J \begin{pmatrix} \rho \bar{W} \\ \rho u \bar{W} + \zeta_z p \\ \rho v \bar{W} + \zeta_r p \\ \rho w \bar{W} + \zeta_\phi \frac{p}{r} \\ \bar{W}(E+p) - \zeta p \end{pmatrix} \quad (4.4)$$

and:

$$I = J \begin{pmatrix} \rho v/r \\ \rho uv/r \\ \rho(v^2 - w^2)/r \\ 2\rho vw/r \\ (E+p)v/r \end{pmatrix} \quad (4.5)$$

where ρ and p are the density and the pressure respectively, E is the total energy and u , v and w are the axial, radial and circumferential velocity components.

The contravariant velocities U , V and W are defined as:

$$\bar{U} = \xi_z u + \xi_r v + \frac{\xi_\phi w}{r} + \xi_t \quad (4.6)$$

$$\bar{V} = \eta_z u + \eta_r v + \frac{\eta_\phi w}{r} + \eta_t \quad (4.7)$$

$$\bar{W} = \zeta_z u + \zeta_r v + \frac{\zeta_\phi w}{r} + \zeta_t \quad (4.8)$$

J is the Jacobian of the inverse transformation:

$$J = x_\xi(y_\eta z_\zeta - z_\eta y_\zeta) - y_\xi(x_\eta z_\zeta - z_\eta x_\zeta) + z_\xi(x_\eta y_\zeta - y_\eta x_\zeta) \quad (4.9)$$

and the metric quantities are:

$$\begin{aligned}
\xi_z &= J^{-1}(r_\eta \phi_\zeta - r_\eta \phi_\zeta) & \eta_z &= J^{-1}(r_\xi \phi_\zeta - r_\xi \phi_\zeta) \\
\xi_r &= J^{-1}(\phi_\eta z_\zeta - z_\eta \phi_\zeta) & \eta_r &= J^{-1}(z_\xi \phi_\zeta - \phi_\xi z_\zeta) \\
\xi_\phi &= J^{-1}(z_\eta r_\zeta - r_\eta z_\zeta) & \eta_\phi &= J^{-1}(z_\zeta r_\xi - r_\zeta z_\xi) \\
\xi_t &= -z_\tau \xi_z - r_\tau \xi_r - \phi_\tau \xi_\phi & \eta_t &= -z_\tau \eta_z - r_\tau \eta_r - \phi_\tau \eta_\phi \\
\zeta_z &= J^{-1}(r_\xi \phi_\eta - \phi_\xi r_\eta) & \zeta_r &= J^{-1}(z_\eta \phi_\xi - \phi_\eta z_\xi) \\
\zeta_\phi &= J^{-1}(z_\xi r_\eta - r_\xi z_\eta) & \zeta_t &= -z_\tau \zeta_z - r_\tau \zeta_r - \phi_\tau \zeta_\phi
\end{aligned} \tag{4.10}$$

The vector I contains the centrifugal and Coriolis force terms due to the propeller rotation. The propeller is assumed to rotate only about the z -axis in the cylindrical coordinate system. Thus, $z_\tau=0$ and $r_\tau=0$ and ϕ is equal to the rotational velocity ω of the propeller. This means that:

$$\zeta_t = -\omega \zeta_\phi \tag{4.11}$$

The spatial derivatives in the equations are replaced by central differences. This means that in NASPROP artificial viscosity must be added explicitly. Furthermore use is made of a first-order accurate implicit time-differencing. Integration of the equations in time will lead to a so-called time-asymptotic solution. The solution becomes steady (in the rotating reference system) when time tends to infinity.

4.1.2 Boundary conditions

The proper application of the boundary conditions for the Euler equations is a very important and difficult subject. During recent years some different techniques have been developed with varying success. It must be understood that using improper boundary conditions can lead to substantial errors in the solution. This process of designing better models for the boundary conditions is still ongoing today.

inflow and outflow boundaries

As described in Chapter 3 at the inflow and outflow boundaries use is made of the theory of characteristics to prescribe the proper number of boundary conditions. If a discretization scheme is used which uses the characteristics theory this discretization technique can also be used in the treatment of the boundaries. Therefore some methods use the same Riemann invariant technique that can be used to calculate the fluxes in the interior of the grid. The characteristic directions belonging to the individual fluxes determine the direction in which the fluxes are discretized. A comparable approach using characteristics is used by Whitfield^[4,6]. A detailed theoretical description of the method is beyond the scope of this report. The reader is referred to Whitfield et al.^{[4,6], [4,7]} for this. Some basics concerning the method are described briefly.

The 3D Euler equations constitute a hyperbolic system of five first-order partial differential equations. Consider the quasi-linear form of the original set of Euler equations expressed in general curvilinear coordinates:

$$\frac{\partial Q}{\partial \tau} + A \frac{\partial Q}{\partial \xi} + B \frac{\partial Q}{\partial \eta} + C \frac{\partial Q}{\partial \zeta} = 0 \quad (4.12)$$

using:

$$\begin{aligned} \xi &= \xi(x,y,z) \\ \eta &= \eta(x,y,z) \\ \zeta &= \zeta(x,y,z) \\ \tau &= t \end{aligned} \quad (4.13)$$

with:

$$A = \frac{\partial F}{\partial Q}, \quad B = \frac{\partial G}{\partial Q}, \quad C = \frac{\partial H}{\partial Q} \quad (4.14)$$

Note that now the source term I is absent because a fixed reference system is used in this case. The eigenvalues of A define the characteristic directions in the t, ξ -plane, the eigenvalues of B define those in the t, η -plane and the eigenvalues of C define those in the t, ζ -plane. The five eigenvalues of each direction can be written as:

$$\begin{aligned} \lambda_k^1 &= \lambda_k^2 = \lambda_k^3 = k_x u + k_y v + k_z w = \theta_k \\ \lambda_k^4 &= \theta_k + c |\nabla k| \\ \lambda_k^5 &= \theta_k - c |\nabla k| \end{aligned} \quad (4.15)$$

and:

$$|\nabla k| = (k_x^2 + k_y^2 + k_z^2)^{1/2} \quad (4.17)$$

In these formulas k can be respectively ξ , η and ζ . c is the speed of sound. Each eigenvalue λ_k^i is associated with a so-called particular characteristic variable $W_{k,i}$ ($i=1..5$), see Whitfield^[4,6]. Each eigenvalue indicates the direction across a plane $K=\text{constant}$ in which information contained in the associated characteristic variable is propagated. Depending on the sign of the eigenvalue the value of the characteristic variable at the boundary must either be specified or can be determined from the solution and does not have to be prescribed. In Whitfield^[4,6] equations for the characteristic variables can be found expressing the conditions at one side of a boundary in those at the other side. If the grid is chosen such that the inflow or outflow boundary is normal to the ξ -axis then the equations in η and ζ directions can be deleted. The boundary conditions are specified on the basis of the remaining five equations for the both

inflow and outflow boundaries.

For subsonic inflow the signs of four eigenvalues are identical and one eigenvalue is of the opposite sign. Consequently four flow variables at the boundary can be expressed in terms of the 'upstream' values of the flow variables and one condition depends on 'downstream' values of the flow variables. In Barton et al. ^{[4.3]. [4.4]} the following boundary conditions are used. The inflow boundary should represent the freestream conditions. Therefore the components of the velocity (u, v and w) are determined using the free-stream value U_∞ . In addition the derivatives of all other quantities are taken zero.

For subsonic outflow the signs of the eigenvalues are reversed. Again four flow variables depend on the 'upstream' values of the flow variables and one variable depends on the 'downstream' values of the flow variables. Therefore four variables can be expressed in terms of the 'upstream' solution and one variable has to be specified. In principle it is possible to specify the static pressure at the outflow boundary. Instead in Barton et al. ^{[4.3]. [4.4]} the radial equilibrium relation was used:

$$\frac{\partial p}{\partial r} = \left(\frac{\rho v_\theta^2}{r} \right)_b \quad (4.18)$$

Here, v_θ is the tangential component of the velocity in the propeller slipstream. The following relations specifying the boundary conditions in terms of the conditions inside of the flow domain can be derived if four characteristic variables are taken constant across the boundary:

$$\left(\rho - \frac{p}{c_0^2} \right)_b = \left(\rho - \frac{p}{c_0^2} \right)_i$$

$$v_b = v_i$$

$$w_b = w_i \quad (4.19)$$

$$\left(\frac{p}{\rho_0 c_0} + u \right)_b = \left(\frac{p}{\rho_0 c_0} + u \right)_i$$

Index 'b' denotes the condition on the boundary of the domain and index 'i' the condition at the last points inside the computational domain. Using above equations the pressure at the boundary can be determined by integration, using a trapezoidal rule, from the maximum value of r (where the pressure is taken to be the free-stream pressure) down to the rotational axis. The density ρ and the velocity component u at the boundary are also easily determined.

For supersonic inflow and outflow the eigenvalues all have the same sign. Therefore at the inflow boundary all five conditions depend on upstream values of the flow variables and need

to be prescribed. At the outflow boundary the opposite is the case. All variables now depend on the solution and are extrapolated from upstream.

It will be clear that discretization of the boundary conditions is only possible if the values of the primitive variables are known at, for example, points $i,j,K+1$ if points i,j,K are the last points in the computational domain. Therefore, implementation of the boundary conditions can be achieved by using a layer of phantom points located just outside the computational domain ^[4.6]. Conditions at these phantom points are determined by extrapolation using the relation:

$$\psi_p = 2\psi_b - \psi_i \quad (4.20)$$

Impermeable surface boundaries

Boundary conditions at the impermeable surfaces can be applied in several ways. These are described next.

The first technique ^[4.3] uses linear extrapolation of the primitive flow variables. At cell faces on solid boundaries the only contribution to the fluxes stems from the pressure and density (only tangential velocity components are present here). The pressure and density are directly extrapolated from the interior to the boundary surface. The tangency condition is enforced by extrapolating the contravariant velocity and setting the appropriate component to zero. Then the physical velocity components u , v and w can be computed from the inverse of equations (4.9)-(4.11). The advantage of this technique is its ease of application. However, it does not represent the real physical behaviour of the flow at the boundary.

The second technique due to Rizzi ^[4.9] uses a so-called normal momentum relation:

$$\rho \bar{q} \cdot (\bar{q} \cdot \nabla) \bar{n} = \bar{n} \cdot \nabla p \quad (4.21)$$

where \bar{n} represents the unit vector normal to the surface. The equation relates the velocity, density and the body geometry to the normal derivative of the pressure. Using the normal momentum relation in general curvilinear coordinates (ξ, η, ζ) , the pressure at the wall can be estimated by using the pressure gradient normal to the surface which can be expressed in terms of the pressure at the cell centres adjacent to the wall.

A third technique is a method which uses the characteristic variables as described previously ^[4.6]. This method provides the most accurate representation of the physical boundary. It can be shown that if there is no flow going through the boundary, the first three eigenvalues are zero, the fourth positive and the fifth negative. Therefore only one condition has to be specified, the condition that there is no flow across the boundary. The five equations (if the surface is parallel to plane $k=\text{constant}$) are again used to express the conditions at the

boundary in the conditions in the interior of the domain. The following equations can be derived which express the variables at the boundary (b) in terms of the variables inside the flow domain (index i):

$$P_b = P_i \mp \rho_0 c_0 (\bar{k}_x u_i + \bar{k}_y v_i + \bar{k}_z w_i) \quad (4.22)$$

$$\rho_b = \rho_i + \frac{P_b - P_i}{c_0^2} \quad (4.23)$$

$$u_b = u_i + \bar{k}_x \frac{P_b - P_i}{\rho_0 c_0} \quad (4.24)$$

$$v_b = v_i + \bar{k}_y \frac{P_b - P_i}{\rho_0 c_0} \quad (4.25)$$

$$w_b = w_i + \bar{k}_z \frac{P_b - P_i}{\rho_0 c_0} \quad (4.26)$$

with:

$$\bar{k}_i = \frac{k_i}{|\nabla k|} \quad (4.27)$$

The proper value of k must be chosen which corresponds with the direction of the normal (ξ, η or ζ) on the body surface. The plus sign in equation (4.22) is used if i is in the negative k -direction from the boundary and the minus sign is used if i is in negative k -direction.

Periodic boundary conditions

As was remarked before, for the quasi-steady modelling technique use is made of the symmetry of the flow field with respect to the rotational axis. This fact can also be used to reduce the size of the physical and computational domains (Figures 4.1.a and 4.1.b). Only one of the passages between two propeller blades needs to be used in the calculations. The solution of the complete flow field is obtained by simply adding copies of the calculated subdomain. It can be seen that by proper mapping of the physical domain a rectangular computational domain can be obtained with two boundary surfaces aligned with the upper and lower surface of the blades (ζ_{\min} and ζ_{\max}). On the blade surfaces the impermeable surface boundary conditions are imposed. On the rest of the surface ζ_{\min} and ζ_{\max} periodic boundary conditions must be imposed. Again use can be made of the symmetry of the flow field by taking the cells at ζ_{\min} as phantom neighbours of ζ_{\max} and vice versa.

4.1.3 Initial condition

For the time-asymptotic solution of the Euler equations it is not very important what initial conditions are specified. Freestream conditions could be imposed or results from a previous calculation.

4.2 Modelling of the unsteady flow due to propeller slipstreams

In cases of propellers at angle of attack or multiple counter-rotating propellers the flow field is truly unsteady and cannot be treated with the quasi-steady modelling technique. In the literature a real time-dependent modelling technique can be found^{[4.6],[4.7]}. A model is used that is valid for non-stationary, non-constant volumes. Later in this section a few remarks will be made about this non-constancy of the volumes (distortion of the grid).

4.2.1 Transformation of the Euler equations

The Euler equations described in Chapter 3 are transformed from a Cartesian reference frame to a body-fitted curvilinear reference system. In this case however no use is made of cylindrical coordinates. The equations are quite similar to the quasi-steady ones, but they are given for the sake of completeness.

Transformation:

$$\begin{aligned}\xi &= \xi(x, y, z, t) \\ \eta &= \eta(x, y, z, t) \\ \zeta &= \zeta(x, y, z, t) \\ \tau &= t\end{aligned}\tag{4.29}$$

The system in Chapter 3 transforms to:

$$\frac{\partial Q}{\partial \tau} + \frac{\partial F}{\partial \xi} + \frac{\partial G}{\partial \eta} + \frac{\partial H}{\partial \zeta} = 0\tag{4.30}$$

where:

$$Q = J \begin{pmatrix} \rho \\ \rho u \\ \rho v \\ \rho w \\ e \end{pmatrix} \quad F = J \begin{pmatrix} \rho U \\ \rho u U + \xi_x p \\ \rho v U + \xi_y p \\ \rho w U + \xi_z p \\ U(e+p) - \xi_t p \end{pmatrix} \quad (4.31)$$

$$G = J \begin{pmatrix} \rho V \\ \rho u V + \eta_x p \\ \rho v V + \eta_y p \\ \rho w V + \eta_z p \\ V(e+p) - \eta_t p \end{pmatrix} \quad H = J \begin{pmatrix} \rho W \\ \rho u W + \zeta_x p \\ \rho v W + \zeta_y p \\ \rho w W + \zeta_z p \\ W(e+p) - \zeta_t p \end{pmatrix} \quad (4.32)$$

with:

$$e = p/(\gamma-1) + \rho(u^2+v^2+w^2)/2 \quad (4.33)$$

and the contravariant velocities:

$$U = \xi_x u + \xi_y v + \xi_z w + \xi_t$$

$$V = \eta_x u + \eta_y v + \eta_z w + \eta_t \quad (4.34)$$

$$W = \zeta_x u + \zeta_y v + \zeta_z w + \zeta_t$$

and the Jacobian of the inverse transformation:

$$J = x_\xi(y_\eta z_\zeta - z_\eta y_\zeta) - y_\xi(x_\eta z_\zeta - z_\eta x_\zeta) + z_\xi(x_\eta y_\zeta - y_\eta x_\zeta) \quad (4.35)$$

and the metric quantities:

$$\xi_x = J^{-1}(y_\eta z_\zeta - z_\eta y_\zeta) \quad \eta_x = J^{-1}(z_\xi y_\zeta - y_\xi z_\zeta)$$

$$\xi_y = J^{-1}(z_\eta x_\zeta - x_\eta z_\zeta) \quad \eta_y = J^{-1}(x_\xi z_\zeta - z_\xi x_\zeta)$$

$$\begin{aligned}
\xi_z &= J^{-1}(x_\eta y_\zeta - y_\eta x_\zeta) & \eta_z &= J^{-1}(x_\zeta y_\xi - y_\zeta x_\xi) \\
\xi_t &= -x_\tau \xi_x - y_\tau \xi_y - z_\tau \xi_z & \eta_t &= -x_\tau \eta_x - y_\tau \eta_y - z_\tau \eta_z \\
\zeta_x &= J^{-1}(y_\xi z_\eta - z_\xi y_\eta) & \zeta_y &= J^{-1}(x_\eta z_\xi - z_\eta x_\xi) \\
\zeta_z &= J^{-1}(x_\xi y_\eta - y_\xi x_\eta) & \zeta_t &= -x_\tau \zeta_x - y_\tau \zeta_y - z_\tau \zeta_z
\end{aligned}
\tag{4.36}$$

This system of equations rewritten, in integral form can be discretized by using a finite-volume method. The ways in which the fluxes at the faces are calculated varies in each of the references on this subject.

The boundary conditions that have to be specified for this type of problem are the same as those for the quasi-steady case. In this case however no use can be made of the axial symmetry and therefore the periodic boundary conditions cannot be used. Problems occur for the internal boundaries of the different blocks. In the next sections the treatment of internal boundaries is described further.

4.2.2 Grid generation for propeller flows

From the computational point of view the major problem in treating time-dependent propeller flows with Euler methods lies in the construction of proper grids. It is obvious that there is a relative motion between the propeller and the airplane. A single stationary grid that wraps around both the propeller and the wing is not possible. It would have to distort considerably in time and the resulting calculations will turn inaccurate after a very short period.

The problems can be overcome by subdividing the space in zones or blocks. Several advantages can be mentioned concerning blocked grids. First of all different regions of interest can be divided into geometrically simpler sub-regions. Grids can then be generated independently for each block using existing grid generator schemes. Relative motion of different parts can be accommodated by restricting the stationary parts in one set of blocks and the moving parts in others. Also local refinement of the grid can be confined to a smaller region (one block). Furthermore the use of multiple blocks can reduce the amount of (expensive) core computer memory. The data of other blocks can be stored on disc.

Certain requirements must be met at the interfaces of different blocks. Across these interfaces information is transferred from one block to the other. The boundary conditions at the interface should be such that the solution of the problem is not influenced by the subdivision. Therefore, some requirements can be formulated. The algorithm used to implement the conditions must be:

- numerically stable
- spatially and temporally accurate
- easily applicable in generalized coordinates
- (kept) conservative so that discontinuities can move from one block to the other.

In the next section the different techniques which are used for treating the interfaces are described.

4.2.3 Interface boundary condition between grid blocks

There are three different approaches to composite gridding of the physical space ^{[4.7],[4.10]}. These are; patched gridding, overlaid gridding and (dynamic) blocked gridding. The different approaches differ in the way in which the interface between the subdomains is treated. The patched-grid approach is a technique where different blocks of generally different topologies (zones) join along common boundaries, see Figure 4.2. In this approach information transfer between different blocks occurs at the interfaces which separate the zones. The second technique is the overlaid technique, see Figure 4.3. In this approach the blocks do not have a common boundary, but overlap instead. In this case information transfer takes place in the overlap region. In the third approach, the blocked gridding approach, is much like the patched grid approach but it does not need interpolation of the information on the interfaces because the spacing of the grid lines of both blocks is equal.

Both patched- and overlaid-grid techniques have their relative advantages and disadvantages. In overlaid grids an interpolation in n dimensions of an n -dimensional flow problem is required. Patched grids require only an $(n-1)$ dimensional interpolation. Furthermore maintaining global conservation with overlaid grids is more difficult to achieve than by using patched grids. The advantages of overlaid grids over patched grids are that this method is more flexible in generating grids and the grids can move more easily relative to each other (no discrete time stepping for proper positioning of the cell faces).

As already stated, the patched-grid method and the overlaid-grid method need interpolations for the transfer of information across block boundaries even when blocks are not in relative motion. The dynamic blocked-grid approach eliminates this requirement. The early version of the method required that the grid spacing (lines) be uniform in the azimuthal direction at the block interface. This eliminates the need for interpolation and considerably simplifies the task of maintaining conservation of the flow properties across block interfaces. The technique is also called an extraction-injection technique because values from within the domain of one block are extracted and then injected (as phantom values) in the adjacent block (Figure 4.4). Note the need for extra interpolation for the case of relative motion between blocks.

A serious drawback of the dynamic blocked grid approach is that permissible time-steps are linked to the grid spacing in the azimuthal direction at the interface (the gridlines stay continuous after each time step. As is stated in Nallasamy et al. ^[4.11] a restriction of the timestep size will lead to errors in 'tracking' the waves that move from one block to the other. A numerical scheme will mistrack the wave differently in both blocks. With 'mistracking' is meant the artificial acceleration or retardation of waves. Hence a "shearing" of the wave might be expected at the interface if large timesteps (increasing such mistracking errors) are chosen. It seems that this will be true each time two computational domains moving relative to one another are "connected" such that the grid time metrics are discontinuous. Thus, the patched grid method, the overlaid grid method and the dynamic blocked grid method with discrete time steps all suffer from this same effect. Another

disadvantage is that if a non-uniform spacing is used between blade rows in the azimuthal direction the spacing must transition to a uniform spacing at the relative-motion block-boundary interface. This because the cells at the boundary between the blocks must be the same size.

In Nallasamy et al. ^[4.11] a number of approaches is taken to eliminate the mistracking problem. The first approach is that of using additional iterations (sweeps of the grid) at each time-level. The objective of this approach is to view each time-level as a quasi steady-state. With this the tracking error is reduced with each iteration count. In ^[4.11] it is observed that using more iterations leads to a better approximation of the fluctuating blade pressure coefficients.

The second approach is obviously the use of smaller time steps. In Janus ^[4.7] another approach is used, the so-called localized grid-distortion (regridding) technique that is aimed at distributing more equally the wave tracking error. This technique does not require uniform spacing in the azimuthal direction at the interface. A region between blade rows is established across the axial block-block boundary and designated as the grid distortion zone. The radial and axial positions of all points within the zone remain constant, only the angular positions is adjusted at each time-level to accommodate the propeller rotations (Figure 4.5). The redistribution of grid points is done by examining the boundary points in axial and circumferential direction and linking a fore-boundary point to an aft-boundary point with a line or Bezier curve and then interpolating to find the new angular positions of the interior points lying on this line. Of course the geometry of the blades must not be distorted. Like the discrete-rotation method, no interpolation of the solution is required at the relative-motion block-boundary interface.

As described in Section 4.2, boundary conditions are implemented in Whitfield ^[4.6] by using phantom points. This technique is also used for transfer of information from one grid block to another. This means that for each block phantom points are defined that lie in each block having common faces with that block. These phantom points are in this case not artificial points but rather the cell-centres of the cells of the adjacent blocks. As the grid is swept during each time-step, the values of the conserved quantities of the preceding time-step in the phantom points are used as the boundary conditions for each grid block.

4.2.4 Initial condition

For the real time-dependent flows the initial condition is important for the development of the flow field. Usually the same initial conditions are specified as in the quasi-steady case, thus the unperturbed flow field. Then the problem is solved for a certain time period in which the flow field starts to develop. After a few rotations of the propeller the influence of the initial condition and the transients fade away and the desired time-dependent flow field is obtained.

4.3 Some results of testcases

In this section the results of some validation testcases are described. It must be mentioned that there are more examples available of propeller flow simulations using Euler methods but they

are performed simply to explore the possibility of the methods ^{[4.12],[4.13]} or to test new ways of treating the block boundary conditions ^[4.7]. The results of these calculations are not validated employing experimental results.

A popular testcase for validating 3D Euler methods in their use for predicting unsteady propeller flows is the Hamilton Standard SR-3 propeller (Figure 4.6) that was used in experiments by Heidelberg and Clark ^[4.1]. This is an eight-blade propeller-spinner-nacelle configuration with highly twisted and highly swept blades. In the experiments unsteady blade pressure distributions were obtained for the SR-3 propeller for a range of Mach numbers at various advance ratios and blade angles. Also the effects of angle of attack were investigated (up to 4°). This testcase is used in Bober ^{[4.2],[4.3],[4.4]} for the quasi-steady modelling technique and in Whitfield ^[4.6] also for the real time-dependent case (at 4° angle of attack). The Mach number was 0.8. The advance ratios ranged from 2.9 to about 3.7.

Comparison of measured and computed (Bober ^{[4.2],[4.3],[4.4]}, and Whitfield ^[4.6]) power coefficients in ^[4.6] show a considerable difference (Figure 4.7). A maximum deviation of 10 percent is no exception. It is stated that refinement of the grid (in ^[4.6]) can substantially improve this result. Comparison shows that computations generally predict swirl angles higher than those measured (Figure 4.8). Explanations for these differences are according to the writers viscous effects and again the coarseness of the grid. It must be mentioned that using the radial equilibrium condition instead of the constant pressure condition at the far field edge has a large positive influence on the prediction of the swirl angle. If this condition is used the differences between calculated and measured angles are in the order of 2 to 3 degrees (maximum swirl angle in the experiments is about 6 degrees). It is therefore concluded that the boundary conditions that are prescribed are very important for the quality of the calculations. Comparison of the surface pressures and their fluctuations (waves) in ^[4.6] at Mach numbers 0.6 and 0.8 for the case of 4° angle of attack leads to the conclusion that the Whitfield method can give very accurate approximations.

Another testcase is a propfan configuration (General Electric-UDF) with counter-rotating propellers Smith ^[4.14] (Figure 4.9). In this article the propfan performance is measured for various advance ratios and free stream angles of attack of 0° and 2°. This testcase is also used in Whitfield ^[4.6]. Because of the counter-rotation the radial condition was not needed at the far-field boundary. Again the power coefficient is overpredicted over the entire range of advance ratios. At high tip speeds (low advance ratio) the computed power coefficient is approximately 15 percent higher, and increases to 20 percent at lower values of the tip velocity (Figure 4.10). Furthermore the calculated results show that the influence of the angle of attack on a propfan is rather small (as is the case in the experiments). It seems that the 2° angle of attack is too small in that respect. If the propulsion efficiency is compared, it seems that at low advance ratios the calculated efficiency is very near the experimental value (Figure 4.11). At higher advance ratios (2.8-3) the calculated efficiency is about 10% higher than the measured efficiency.

In Nallasamy ^[4.11] a 3D Euler method was used to predict the blade pressures for input into a time domain acoustic calculation for a SR-7A propeller over a range of loadings investigated in the NASA Lewis 9- by 15 foot Anechoic Wind Tunnel. The predicted power

coefficients were in reasonable agreement with the measured values for three blade angles (loadings) over a range of advance ratios. While fundamental tone agreement between data and predictions is good at the lowest loading case, there is an increasing tendency to underpredict as the loading is increased. When a propeller is operating appreciably off-design such as at takeoff, a leading-edge vortex that merges with the tip vortex is expected to form. The phenomenon is similar to the vortex structure on a delta wing aircraft at high angle of attack. If the associated loading distribution is not accounted for in the model, errors in the aerodynamic performance and/or the tone noise level predictions will result. Failure to adequately define such a complex propeller loading distribution is the suspected cause of the underprediction of the tone noise at high loading. It remains to be investigated whether the inviscid Euler method solution accurately captures the main features of the vortex flow and, therefore, is useful for acoustic predictions at conditions such as take-off.

In Nallasamy ^[4.15] the SR-7L propfan propeller is used to compare results from a finite-difference Euler method (NASPROP code) with results from a finite-volume Euler method (Denton's method) with experimental results. Both methods use the quasi-steady modelling technique and use central differencing to discretize the system of equations. Therefore, the artificial dissipation terms must be added explicitly by the user. Both transonic and low subsonic cases are treated at zero angle of attack. In general, both techniques predict the blade pressure distributions fairly well for the range of Mach numbers between 0.2 to 0.78. The finite-difference method predicts a trailing-edge shock at Mach numbers of about 0.78 unlike the finite-volume method and the experiments. For the low Mach number (0.2) the predictions were best for the low loading case. In the high-loading case a leading-edge vortex is formed but this vortex is not captured by either Euler method. It must be concluded that proper grid refinement and improvements in added dissipative terms are required in this case. The same SR-7L propeller was used in Kobayakawa ^[4.16] but now using a more advanced differencing scheme (TVD scheme) that is better capable of capturing discontinuities.

4.4 Wake development as a part of the iteration process

If accurate information of the flow in the propeller wake is required it is essential that the proper shape of the wake forms in the solution of the Euler method. As was described in Chapter 2, the propeller wake consists of initially helical shaped vortex sheets which are distorted as they are transported downstream. It is therefore essential that the Euler method is able to capture these vortex sheets. Obviously the grid must be enough refined so that the vortex sheets can be captured in detail. This is difficult because the vortex sheets are moving in time. Therefore the complete slipstream must be gridded with many cells, which is very expensive in calculation time, or a grid adaptation technique must be used that modifies the grid after a certain number time-steps so that the highest resolution is moved to a new region with large values of the vorticity. According to the author there are no applications of this grid-refinement technique yet in the field of numerical propeller slipstream simulation.

A second remark about the capturing of the wake can be made regarding the numerical dissipation which is generated in the Euler methods. The explicit addition of numerical

dissipation in the case of central differencing does not guarantee automatically the proper level of dissipation and therefore of the proper representation of the propeller slipstream. In that respect upwind schemes have shown to capture the discontinuities more crisply. However, a drawback of the upwind schemes is that although they automatically generate numerical dissipation, the level of this dissipation depends on the grid quality.

A final remark can be made regarding the capturing of the leading-edge vortex in Euler methods. The development of this vortex for high loading cases of propellers with a highly swept blade is due to the separation of the flow at the (relatively sharp) leading edge. Therefore it is a viscous problem. It is generally accepted now that the current Euler methods are able to capture the leading-edge vortex caused by flow separation at 'aerodynamically sharp' edges accurate enough so that accurate pressure calculations on the blades and in the slipstream can be obtained. This under the condition of a sufficient size of the vortex (vortex not engulfed in the boundary layer).

5 Propeller simulation by actuator-disc representation

The basic goal of a propeller is to add an amount of momentum flux to a certain amount of air with the object to generate thrust. Often the concern of the designer is to focus on the interference effects generated on the airframe rather than the details of the blade-to-blade flow field of a propeller. In that case the propeller slipstream might be considered as a time-averaged flow field. This in contrast with the time-dependent or quasi time-dependent modelling approach of propeller slipstreams as discussed in Chapter 4. In the next sections this time-averaged modelling technique is described.

5.1 Introduction of actuator disc concept

The time-averaged modelling of the slipstream uses the so-called the actuator disc representation of the propeller. The propeller is considered as an infinitely thin disc which discontinuously increases the momentum and energy of the flow, i.e., changes the magnitude of the velocity components and other flow variables. In the actuator disc concept the exact shape of the propeller blades is not relevant. Only the forces exerted by the propeller on the flow are important. This concept significantly simplifies the modelling task and consequently saves computer-calculation time and costs, which of course are very important aspects in the aircraft design process.

Application of the actuator disc concept hinges on imposing proper boundary conditions on the solution of the conservation equations. The Euler equations allow solutions with distributed vorticity and discontinuities like shockwaves and vortex sheets. The propeller plane can also be regarded as a discontinuity surface.

Because a system of five conservation law equations is used, five jump conditions are available to apply to the propeller disc. The jump conditions across the actuator disc must accurately simulate propeller loading and swirl effects. Solving the conservation equations with the imposed boundary conditions by discretization techniques then automatically incorporates the time-averaged effect of the propeller on the flow field.

Generally the propeller disc is represented by a number of rectangles along a computational grid plane. Obviously a grid type should be chosen with which it is possible to embed the actuator disc properly in the grid. It is evident that the fineness and quality of the discretization of the space around the disc and of the disc itself will influence the quality of the simulation of the effect of the propeller on the time-averaged flow field. A large number of cells near the propeller plane will lead to a better approximation of the flow induced by the disc.

The actuator disc concept does not directly use the aerodynamic shape of the propeller. A separate computational method or the results of experiments have to be used to supply the

proper boundary conditions. Chapter 2 deals with propeller analysis methods.

5.2 Boundary conditions

Along the disc, properly chosen boundary conditions for the conserved variables ($\rho, \rho u, \rho v, \rho w, \rho E$) are needed in order to simulate effects, like the introduction of swirl, of the propeller on the flow field. These boundary conditions are obtained by expressing the conserved variables at both sides of the disc in terms of the conserved variables at other grid points. In this way, the boundary conditions can be discretized and included in the system of first-order partial differential equations. Because of the boundary (jump) conditions the conserved variables will vary discontinuously across the disc.

Basically three different approaches can be followed to calculate the jumps in the variables across the disc ^[5.1]. These are:

- specification of the distribution of force and work delivered by the propeller to the flow
- specification of flow conditions on the downstream side of the disc
- introduction of source terms in the form of body forces in the governing equations

These three methods are described in the next sections.

5.2.1 Boundary conditions using prescribed work and force

The first method assumes that information is available about the distribution over the propeller disc of the force F and of the work Q exerted by the propeller on the air. The Euler equations are applied to an infinitesimal domain with volume V , bounded by surface ∂V that contains a part of the actuator disc with surface ∂S to express the flow variables at the downstream side of the disc in terms of the flow variables at the upstream side (Figures 5.1. and b for the 2D case). This is achieved as follows using the Euler equations.

mass conservation:

$$\frac{\partial}{\partial t} \iiint_V \rho dV + \iint_{\partial V} \rho \vec{u} \cdot \vec{n} dS = 0 \quad (5.1)$$

Because a time-averaged approach is used the time-dependent part can be dropped resulting in the following jump condition across the disc:

$$[[\rho u_n]] = 0 \quad (5.2)$$

or expressed in upstream (1) and downstream (2) terms:

$$\rho_1 u_{n_1} = \rho_2 u_{n_2} \quad (5.3)$$

Here u_n is the velocity component normal to the actuator disc.

Momentum equation:

$$\frac{\partial}{\partial t}(m\bar{u}) = \frac{\partial}{\partial t} \iiint_V \rho \bar{u} dV + \int_{\partial V} \rho \bar{u} (\bar{u} \cdot \bar{n}) dS = \bar{F}_s \quad (5.4)$$

The force vector \bar{F}_s contains a pressure part and a part which is introduced by the propeller (external force). The viscous part of \bar{F}_s is neglected. Thus, \bar{F}_s can be written as:

$$\bar{F}_s = \int_{\partial S} [-p\bar{n} + \bar{F}\bar{n}] dS \quad (5.5)$$

with p the static pressure and \bar{F} a force per unit area. Again the time-dependent part is ignored resulting in the following equations for the jump conditions in the directions normal to and in the plane of the actuator disc (Figure 5.2):

$$\rho_2 u_{n_2}^2 + p_2 = \rho_1 u_{n_1}^2 + p_1 + (\bar{F} \cdot \bar{n}) \quad (5.6)$$

$$\rho_2 u_{n_2} \bar{u}_{t_2} = \rho_1 u_{n_1} \bar{u}_{t_1} + \bar{F}_t \quad (5.7)$$

with:

$$u_n = \bar{u} \cdot \bar{n} \quad (5.8)$$

$$\bar{u}_t = \bar{u} - (u \cdot \bar{n}) \bar{n} = \bar{n} \times (\bar{u} \times \bar{n}) \quad (5.9)$$

$$\bar{F}_t = \bar{n} \times (\bar{F} \times \bar{n}) \quad (5.10)$$

Energy equation:

$$\frac{\partial}{\partial t} \iiint_V \rho E dV + \int_{\partial V} \rho E (\bar{u} \cdot \bar{n}) dS = - \int_{\partial V} p \bar{u} \cdot \bar{n} dS + \int_{\partial S} Q dS \quad (5.11)$$

Here Q represents the distributed work (in J/m^2) exerted on the flow by the propeller. Again the first term is dropped. Using:

$$H = E + \frac{p}{\rho} = \frac{\gamma}{\gamma-1} \frac{p}{\rho} + \frac{1}{2} U^2 \quad (5.12)$$

it follows for the jump over the disc:

$$[[\rho u_n H]] = Q \partial S \quad (5.13)$$

or expressed in upstream (1) and downstream (2) terms:

$$\rho_2 u_{n_2} H_2 = \rho_1 u_{n_1} H_1 + Q \delta S \quad (5.14)$$

Using equation (5.3) the density ρ_2 can be expressed in terms which depend on the prescribed work and flow variables which can be extrapolated from the solution.

$$H_1 + \frac{Q \delta S}{\rho_2 u_{n_2}} = H_2 = \frac{\gamma}{\gamma - 1} \frac{P_2}{\rho_2} + \frac{1}{2} U_2^2 \quad (5.15)$$

$$\rho_2 = \frac{\gamma}{\gamma - 1} \frac{P_2}{\left(H_1 + \frac{Q \delta S}{\rho_2 u_{n_2}} - \frac{1}{2} U_2^2 \right)} \quad (5.16)$$

Using the equations described above, the boundary conditions at both sides of the actuator disc can be determined. The number of boundary conditions which have to be specified depend on the nature of the boundary as has been described in Chapter 4. The upstream side of the disc is a subsonic outflow boundary where only one boundary condition has to be prescribed and the other four can be obtained by extrapolation from the solution (boundary condition is discretized by using the values of the variables at neighbouring (upstream) cells). At the downstream side the disc is an inflow boundary and four boundary conditions need to be prescribed and one depends on the solution.

At the downstream side of the disc velocity U_2 , defined by:

$$U_2^2 = u_2^2 + v_2^2 + w_2^2 \quad (5.17)$$

can be obtained by extrapolation from the values of U_2 at downstream grid points. Here u_2, v_2, w_2 are the velocity components in an arbitrary coordinate system. Using equations (5.6) and (5.7) with density ρ_2 specified by equation (5.16) the conservative variables ($\rho, \rho u, \rho v, \rho w, \rho E$) at the downstream side can be expressed in terms of the upstream conservative variables and the prescribed force and work distributions across the propeller disc. The mass flux $\rho_2 u_{n_2}$ at the downstream side, which according to equation (5.3) is equal to $\rho_1 u_{n_1}$, can now be calculated and used as a boundary condition for the upstream side. The other four conserved variables at the upstream side are extrapolated from upstream.

5.2.2 Boundary conditions using prescribed flow conditions

The second method assumes that the distribution of total pressure p_t , total temperature T_t and the swirl angle δ are known at the downstream side of the disc. Therefore, instead of specifying forces and work the jump in the total pressure and temperature and the change in the direction of the flow is specified.

Like in 5.2.1 the the velocity U_2 is obtained by extrapolation of the solution from downstream. Then the Mach number M_2 can be computed with the prescribed total

temperature T_{t_2} using:

$$M_2^2 = \frac{\frac{2}{\gamma-1} U_2^2}{\frac{2\gamma RT_{t_2}}{\gamma-1} - U_2^2} \quad (5.18)$$

which can be obtained by combining the following two formulae:

$$T_2 = \frac{T_{t_2}}{(1 + \frac{\gamma-1}{2} M_2^2)} \quad (5.19)$$

$$M_2^2 = \frac{U_2^2}{a_2^2} = \frac{U_2^2}{\gamma RT_2} \quad (5.20)$$

The static pressure p_2 is obtained using:

$$p_2 = \frac{p_{t_2}}{(1 + \frac{\gamma-1}{2} M_2^2)^{\frac{\gamma}{\gamma-1}}} \quad (5.21)$$

Next, the velocity components u_2 , v_2 and w_2 can be computed using U_2 and δ . The density ρ_2 can be obtained using (5.21) and the equation of state:

$$\rho_2 = \frac{p_2}{RT_2} \quad (5.22)$$

Using the above equations, the conserved variables can be expressed in terms of the solution and the prescribed values for p_{t_2} , T_{t_2} and δ . Again the normal mass flux ρu_{n_2} can be obtained and is prescribed at the upstream side of the disc.

In some cases in the literature the effect of the boundary layer on the nacelle is modelled by prescribing a zero jump in the total enthalpy ($H_2=H_1$) in the neighbourhood of the nacelle. This is also the case for the tip of the propeller where no momentum is added to the flow.

Supersonic flow conditions

In the case of supersonic inflow conditions, which may arise in the flow around a propfan, a special treatment of the boundary conditions must be followed. If M_1 is greater than 1, flow conditions upstream of the propeller are not influenced by downstream conditions. In that case all flow variables depend on upstream flow conditions and can therefore be obtained by extrapolating from upstream. Instead of prescribing the work Q in the first method or the total temperature T_{t_2} in the second method the mass flux obtained from the upstream values of the flow variables can be used as a boundary condition on the downstream side of the propeller

disc. If both upstream and downstream flow conditions are supersonic the described are no longer valid.

5.2.3 Addition of source terms to the Euler equations

The third method is a method used by Jameson^[5.2]. The method is quite similar to the first method except that here the distributed force and work applied by the propeller are directly inserted in the Euler equations instead of used as boundary conditions. The force and work are introduced as source terms in the form of body forces in the governing equations. The 3-D time-dependent Euler equations can be written as:

$$\iiint_V \frac{\partial \bar{G}}{\partial t} dV + \iint_{\partial V} (\bar{F} \cdot \bar{n}) dS - \int_{\partial V} \bar{B} dS = 0 \quad (5.23)$$

with:

$$\begin{aligned} \bar{G} &= [\rho, \rho u, \rho v, \rho w, \rho E]^T \\ \bar{F}_x &= [\rho u, \rho uu + p, \rho vu, \rho wu, \rho(E + \frac{p}{\rho})u]^T \\ \bar{F}_y &= [\rho v, \rho uv, \rho vv + p, \rho wv, \rho(E + \frac{p}{\rho})v]^T \\ \bar{F}_z &= [\rho w, \rho uw, \rho vw, \rho ww + p, \rho(E + \frac{p}{\rho})w]^T \\ \bar{B} &= [0, \rho \bar{f}_x, \rho \bar{f}_y, \rho \bar{f}_z, \rho(\bar{f}_x u + \bar{f}_y v + \bar{f}_z w)]^T \end{aligned} \quad (5.24)$$

Here f_i are the components of the distributed force \bar{F} and $f_i u_i$ is the distributed work Q . Instead of using boundary conditions in this method the equations are modified to include the terms B . In this way the equations seem to include source terms. In^[5.4] a further description is given of these source terms. Generally the terms can be written as a function of the lift and drag coefficients C_l and C_d of the propeller blade, the angle of attack of the propeller blade with respect to the relative velocity vector, the absolute velocity of the fluid at the instantaneous blade location (R, Θ, t) , some geometric properties of the blade, and some flow parameters like the Mach number or the Reynolds number. If unsteady and viscous effects are neglected and the aerodynamic characteristics of the blade sections are known, the source terms can be easily calculated without the need of a separate propeller analysis method. The source terms then evolve as integral part of the solution.

In Jameson^[5.2] use is made of experimentally obtained data to calculate the force terms \bar{f} . The thrust was imposed in the calculations by introducing the same jump in total pressure as measured in the experiments. Force components in the plane normal to the direction of the thrust vector were chosen such that the same level of swirl was obtained as was measured in the experiments. Variation in the stress vector \bar{f} proportional to the square of the distance from the centre of the propeller was used to appropriately simulate swirl variation in radial direction.

5.3 Comparison of the methods

A few remarks can be made about the different choices of imposing the boundary conditions. First of all, the methods are theoretically identical. So a choice must be made on grounds of ease of implementation of the methods.

The advantage of the first method is that the effect of angle of attack and sideslip can be simulated more naturally through the input of normal force and side force distributions along the propeller disc. This approach is followed in Yu ^[5.3]. Of course the propeller model that is used must be able to calculate these force distribution. In the literature however few cases are found where asymmetrical flow conditions were included. Asymmetrical flow conditions are often modelled by simply adding a transverse velocity component to the symmetrical flow field. One of the attempts to include the effect of angle of attack can be found in Schipholt ^[5.5]. A propeller-spinner-nacelle configuration was used to validate an Euler method using an actuator disc representation of the propeller disc. In the testcase two different propeller codes are used that supply the boundary conditions for the actuator disc. The first one is a method based on the blade element theory and the second is a vortex lattice method. Time-dependent propeller loading results were obtained through a large number of calculations. These calculations are performed before the actual solution of the Euler equations. The shape of the wake that was used in both propeller models was prescribed beforehand. Averaged values of the load distribution were deduced from the time-dependent results of both models.

The advantage of the second method lies in the ease of inserting experimentally obtained data. For the purpose of validation often experiments are used. Then the exact aerodynamic properties of the propeller can be obtained and used as jump conditions. Obtaining force distributions from experiments seems very difficult if not impossible.

Some drawbacks of the third method can be mentioned. First of all this methods appears to require rewriting of parts of the CFD-code because it uses modified equations. Modification of existing codes could be more time-consuming then using the standard boundary conditions. Also as described in Yu ^[5.1], oscillatory solutions are usually obtained near the propeller region, especially for heavily loaded propellers when the source terms are relatively large.

5.4 Simulation of counter rotating propellers

Counter-rotating propellers can also be modelled by using an actuator disc. Because the second propeller removes the swirl from the flow that is generated by the first propeller, some simplifications can be made. First of all, the two propellers can be effectively modelled by a single actuator disc. Secondly in the idealized case, the swirl is completely removed by the second propeller. Then the assumption can be made that the jump in the circumferential components of the velocity across the disc is zero. Thirdly, it can be assumed that the jump in the radial velocity is also zero. What remains is only a jump in stagnation enthalpy (the energy) of the flow.

6 Conclusions

In this report a description is given of the application of Euler methods to modelling the flow fields generated by propellers. It has been argued that these advanced design tools will be needed in the design process of future generation civil aircraft that will be powered by new highly efficient propeller propulsion systems. Proper integration of the powerplant will eliminate the adverse interference effects between propeller and the airframe.

The next generation propulsion systems will be geometrically complex and will operate at high subsonic speeds. Modern propeller blades will have considerably higher disc loading and will have to operate at transonic conditions. The relatively simple and computational inexpensive classical propeller modelling methods cannot be used for these new propellers because these propellers are not within the range of applicability of these methods. They also cannot handle off-design conditions very well.

In this report an introduction is given into the general layout of the propeller and its impact on the air that is flowing through it. The development is reviewed of propeller development starting with the momentum theory of Froude and ending with the most complete analytical model that is available, the vortex theory of Theodorsen. Next, the theory behind Euler methods is described. It is explained that the power of Euler methods in modelling propeller flows lies in the fact that their solution automatically includes the propeller slipstream, i.e. the need for a separate propeller wake model is eliminated.

In this report two different ways of modelling the propeller slipstream using Euler methods are described. The first one is the time-dependent modelling and the second one is the time-averaged modelling method. Time-accurate modelling is required if detailed information is needed of the flow in the direct neighbourhood of the propeller blades for example for use in structural or noise analysis. If the designer is only interested in the general interference effects between propeller and airframe use can be made of the time-averaged approach using an actuator representation of the propeller.

In both cases the proper prescription of the boundary conditions for the Euler equations is essential for obtaining a meaningful solution of the problem. In this report some different approaches are described that can be found in literature. In case of the time-averaged simulation extra boundary conditions are needed to prescribe the proper jump conditions at the actuator disc. These jump conditions will have to be supplied by a separate propeller analysis method because the actual propeller model is not included in the Euler model.

Instrumental in proper 'capturing' of the propeller wake is the numerical dissipation added implicitly or explicitly to the discretized system of equations. The quality of the approximation of the flow field is determined by the quality of the computational grid and, when applicable, by the level of artificial dissipation required to let the solution procedure converge. Research is still ongoing at this moment on the subject of designing better

numerical schemes that will guarantee a high quality solution.

Another important requirement for proper slipstream capturing is the fineness of the computational grid. Adapting grids are to be preferred that refine the grid in areas where the flow conditions change rapidly. In case of time-dependent modelling of the propeller complications arise concerning the motion of the propeller and slipstream. A description is given of some solutions that are used for this problem. Adapting grids should be used that follow the vorticity in the slipstream as it moves downstream.

The results of a number of propeller simulations using Euler methods are described. Although the general trends are predicted well, in some cases still large discrepancies can be found between calculated and experimentally obtained pressure distributions, thrust and propulsive efficiency. In some cases these discrepancies can be traced back to the grid quality (no applications of adapting grids have been found), the numerical schemes used and the neglect of the physical viscosity. Also the proper capturing of the leading-edge vortex that develops at the leading-edge of highly loaded, highly swept propeller blades can sometimes be a problem. At this time however it is generally accepted that Euler methods are capable of capturing strong leading-edge vortices, but only if the grid quality is accurate. Weak vortices are more difficult to capture because viscous effects often dominate these flow regions.

References

Chapter 1

- [1.1] Heyma, P.M. "A review of propeller interference effects and modelling techniques", Internal Report LSW 96-1, Delft University of Technology, Netherlands, 1996.
- [1.2] Dugan, J.F., Gatzen, B.S., Adamson, W.M., "Propfan propulsion its status and potential", SAE-780995, 1978.
- [1.3] Grieb, H., Eckardt, D., "Turbofan and propfan as basis for future economic propulsion concepts", AIAA-86-1474 Oct. 1986.
- [1.4] Fulton K., "The propfan...what future now?", Air International, vol. 38, No. 2, Feb. 1990.
- [1.5] Edward J. Hall, Robert A. Delaney, "3D Euler analysis of ducted propfan flowfields", Indianapolis, USA.

Chapter 2

- [2.1] Black, D.M., "Cascade corrections to isolated airfoil data", Internal Correspondence, Hamilton Standard, AR1401, 1974.
- [2.2] Egolf, T.A. et al., "An analysis for high speed propeller nacelle aerodynamic performance prediction", Vol. 1, NASA CR-169450, 1979.
- [2.3] Johnston R.T., Sullivan, J.P., "Unsteady wing surface pressures in the wake of a propeller", AIAA 92-0277, 1992.
- [2.4] Marshall, J.S., "Vortex cutting by a blade, Parts I: General theory and a simple solution", AIAA Journal Vol.32, No.6, June 1994.
- [2.5] Marshall, J.S., "Vortex cutting by a blade, Parts II: computations of vortex response", AIAA Journal Vol.32, No.7, July 1994.
- [2.6] Fogerty, L.E., "The laminar boundary layer on a rotating blade", J.Aero-sci., vol. 18, no. 4, pp 247-252 Sep. 1951.
- [2.7] McCroskey, W., Gadd, G., "Laminar boundary layers on helicopter rotors in forward flight", AIAA Journal, Vol. 6, (10), Oct. 1968.
- [2.8] Narramore, J., Sanker, L., Vermeland, R., "Navier Stokes calculations on inboard Δ delay due to rotation, AIAA Journal of Aircraft, Vol. 29, (1), Jan. 1992.

- [2.9] Corrigan, J.J., Schillings, J.J., "*Empirical model for stall delay due to rotation*", Bell Helicopter Textron Inc., Fort Worth, Texas, USA.
- [2.10] Heyma, P.M. "*A review of propeller interference effects and modelling techniques*", Internal Report LSW 96-1, Delft University of Technology, Netherlands, 1996.
- [2.11] Glauert, H., "*Airplane propellers*", in *Aerodynamic Theory*, Volume 4, Durand, W.F., ed. (J. Springer, Berlin, 1935).
- [2.12] Goldstein, S., "*On the vortex theory of screw propellers*", Royal Society Proceedings, Series A, Vol. 123, London, 1929.
- [2.13] Wentzel, C.M., "*The application of the finite element method to an aerodynamic problem specific to propeller design*", report No.LR-614, Delft University of Technology, March 1990.
- [2.14] Eshelby, M.E., "*On the aerodynamics of installed propellers*", AGARD CP-366, paper 8, 1984.
- [2.15] Theodorsen T., "*Theory of propellers*", McGraw-Hill book company, Inc., 1948.
- [2.16] Schouten, G., "*Static Pressure in the Slipstream of a Propeller*", AIAA 82-4055, 1982.

Chapter 3

- [3.1] Boerstael, J.W., "*A survey of numerical methods for the calculation of inviscid, possibly rotational Euler flows around aeronautical configurations*", NLR TR 83130 U.
- [3.2] Jameson, A., Schmidt, E., Turkel, E., "*Numerical solution of the Euler equations by finite volume methods using Runge-Kutta time stepping schemes*", AIAA 81-1259, 1981.
- [3.3] Warsi, Z.U.A., "*Fluid Dynamics: Theoretical and Computational Approaches*", Department of Aerospace Engineering Mississippi State University, 1993
- [3.4] Osher, F., Solomon, F., Math. Comp., "*Upwind differences for hyperbolic systems of conservation laws*", 38:339-374, 1982.

Chapter 4

- [4.1] Heidelberg, L.J., Clark, B.J., "*Preliminary results of unsteady blade surface pressure measurements for the SR-3 propeller*", AIAA Paper No. 86-1893, July 1986.

- [4.2] Bober, L.J., Chaussee, D.S., Kutler, P., "Prediction of high speed propeller flow fields using a three-dimensional Euler analysis", AIAA Paper No. 83-0188, January 1983.
- [4.3] Barton, J.M., Yamamoto, O., and Bober, L.J., "Inviscid analysis of advanced turboprop propeller flow fields" , AIAA 85-1263, July 1985.
- [4.4] Yamamoto, O., Barton, J.M., and Bober, L.J., "Improved Euler analysis of advanced turboprop propeller flows", AIAA 86-1521, June 1986.
- [4.5] Beam, R.M and Warming, R.F., "An implicit finite-difference algorithm for hyperbolic systems in conservation law form", Journal of Computational Physics. Vol. 22, pp 87-110, 1976.
- [4.6] Whitfield, D.L., Swafford T.W., Janus, J.M., Mulac, R.A., Belk, D.M., "Three dimensional unsteady Euler solution for propfans and counter-rotating propfans in transonic Flow, AIAA paper 87-1197, 1987.
- [4.7] Janus J.M., Whitfield, D.L., "Counter-rotating propfan simulation which feature a relative motion multiblock grid decomposition enabling arbitrary time step", AIAA 90-0687, 1990.
- [4.8] Nallasamy, M., Clark, B.J., Groeneweg, J.F., "Euler analysis of the three-dimensional flow field of a high speed propeller: boundary condition effects", Journal of Turbomachinery, Vol.109, No.3, pp332-339, July 1987.
- [4.9] Rizzi, A., "Numerical implementation of solid-body boundary conditions for the Euler equations", ZAMM 58, pp301-304, 1978.
- [4.10] Madavan, N.K., Rai, M.M., "Computational analysis of rotor-stator interaction in turbomachinery using zonal techniques", edited by Henne, P.A., "Applied Computational Aerodynamics", Vol. 125.
- [4.11] Nallasamy, M., Woodward, R.P., Groeneweg, J.F., "High-speed propeller performance and noise predictions at take-off/landing conditions" AIAA Paper 88-0264, Jan. 1988.
- [4.12] Janus, J.M., Whitfield, D.L., Horstman, H.Z., "Computation of the unsteady flowfield about a counterrotating propfan cruise missile", AIAA-90-3093-CP, 1990.
- [4.13] Nallasamy, M., Groeneweg, J.F., "Unsteady analysis of the flow field of a propfan at an angle of attack", AIAA-90-0339, 1990.
- [4.14] Smith, L.H., "Aerodynamic performance tests of unducted fan models", presented at the Advanced Turboprop Workshop, NASA Lewis Research Center, Cleveland, Ohio, Nov. 5-6, 1986.

- [4.15] Nallasamy, N., Yamamoto, O., Warsi, S., Bober, L.J., "*Large-scale advanced propeller blade pressure distributions: prediction and data*", Journ. of Propulsion vol. 7. pp 452-461, May 1991.
- [4.16] Kobayakawa, M., Takaki, R., Kawakami, Y., Metzger, F.B, "*Predicted pressure distribution on a propfan blade through Euler analysis*", Journ. of Aircraft, Vol.29, No. 4, July-Aug 1992.

Chapter 5

- [5.1] Yu, N.J., Chen, H.C., "*Flow simulations for nacelle-propeller configurations using Euler equations*", Boeing commercial airplane company, Seattle, Washington, AIAA-84-2143, 1984.
- [5.2] Jameson, A., Whitfield, D.L., "*Three-dimensional Euler equation simulation of propeller-wing interaction in transonic flow*", AIAA-83-0236, 1983.
- [5.3] Yu, N.J., Kusunose, K., Chen, H.C., Sommerfield, D.M., "*Flow simulations for a complex airplane configuration using Euler equations*", Boeing Commercial Airplane Company Seattle, Washington, AIAA-87-0454, 1987.
- [5.4] Ganesh Rajagopalan, R., Frye, R.R., "*Navier Stokes analysis of the performance a flow field of single and counter-rotating propellers*", AIAA-88-3638-CP, 1988.
- [5.5] Schipholt, G.J., Voogt, N., van Hengst, J., "*Investigation of methods for modelling propeller-induced flow fields*", AIAA 93-0874, 1993.

This page is intentionally left blank

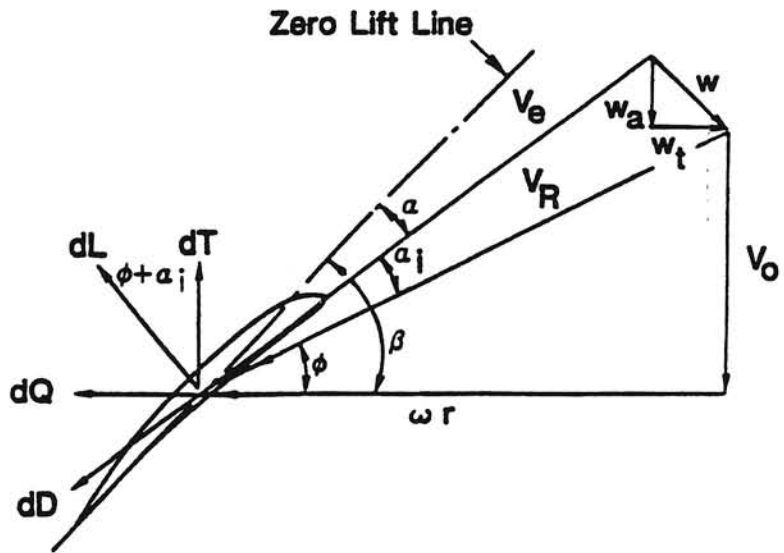
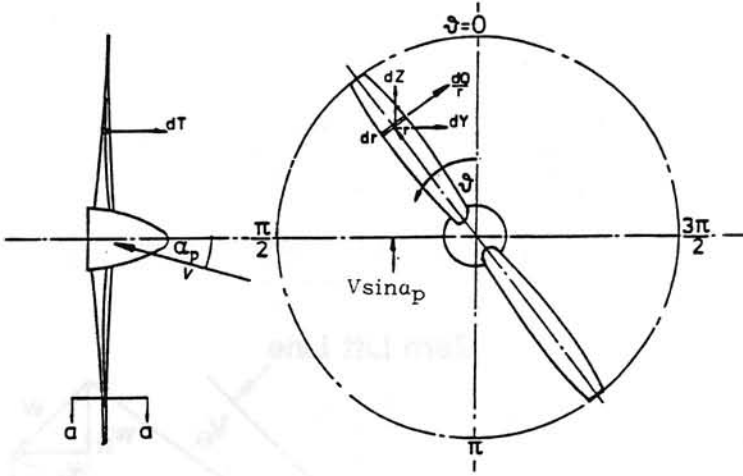


Fig 2.1 Blade element velocity diagram for propeller in symmetric free flow



Propeller Section a-a.

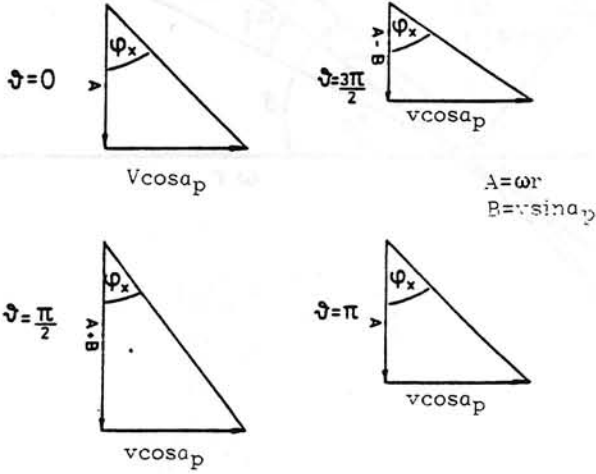


Fig 2.2 Velocity vectors of propeller at angle of attack

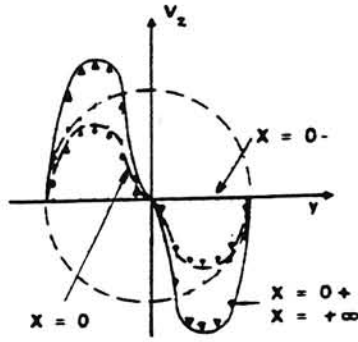


Fig 2.3 Circumferential velocity induced by propeller wake in propeller plane ($x=0$) and in the plane at infinity ($x=\infty$)

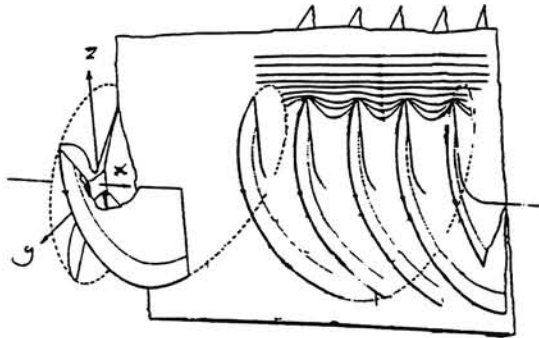


Fig 2.4 Crossflow in radial direction in the x-z plane

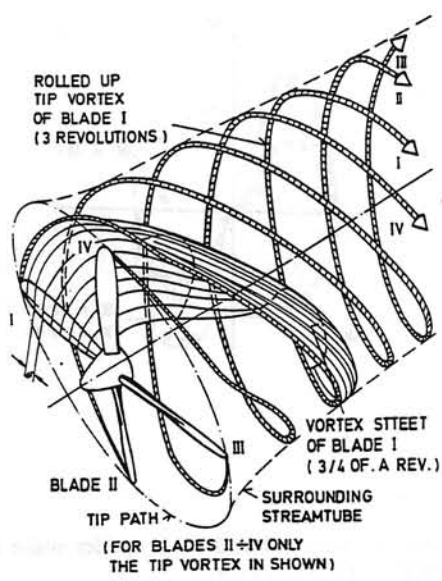


Fig 2.5 Roll-up of the vortex sheet into a tip vortex

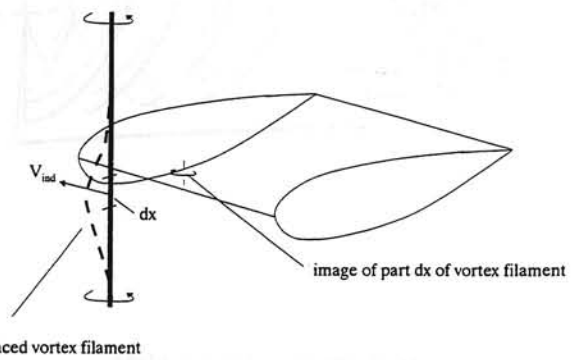


Fig 2.6 The image vortex effect

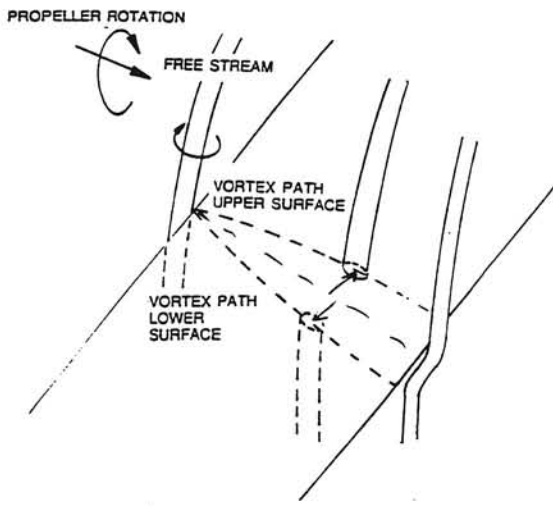


Fig 2.7a The shearing phenomenon of the tip vortex

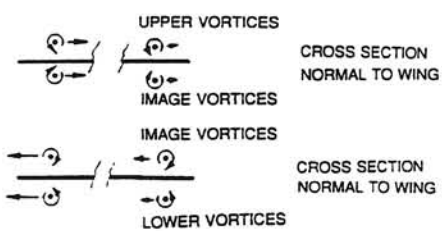


Fig 2.7b Image vortex components in chordwise direction at the upper and lower side of the wing (cross section normal to wing in spanwise direction)

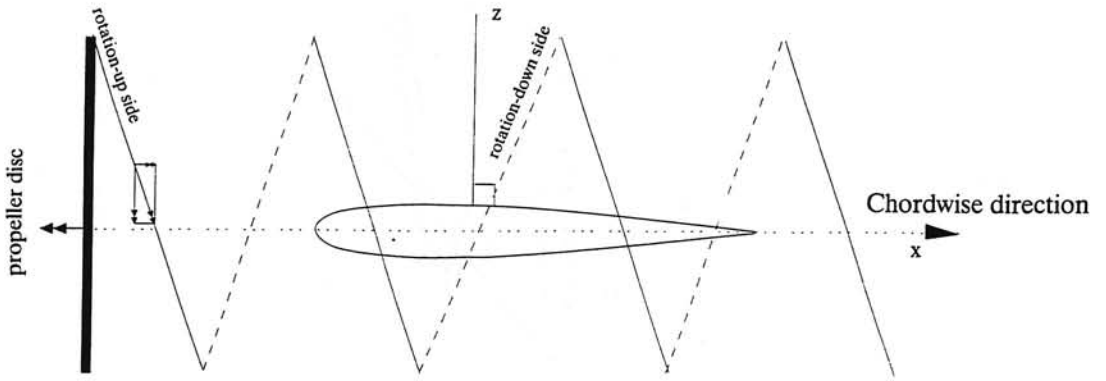


Fig 2.8.a Tip vortex components in x-z plane at low angle of attack

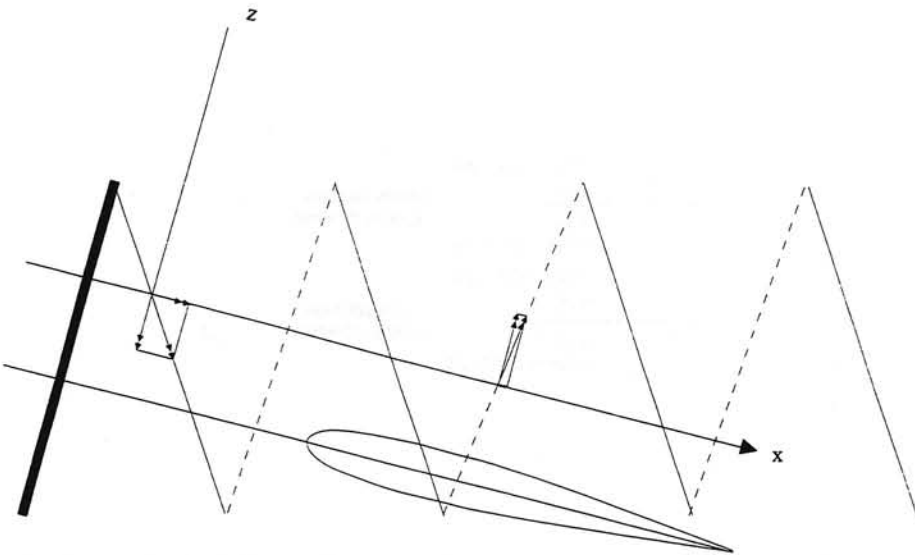


Fig 2.8.b Tip vortex components in chordwise direction at high angle of attack

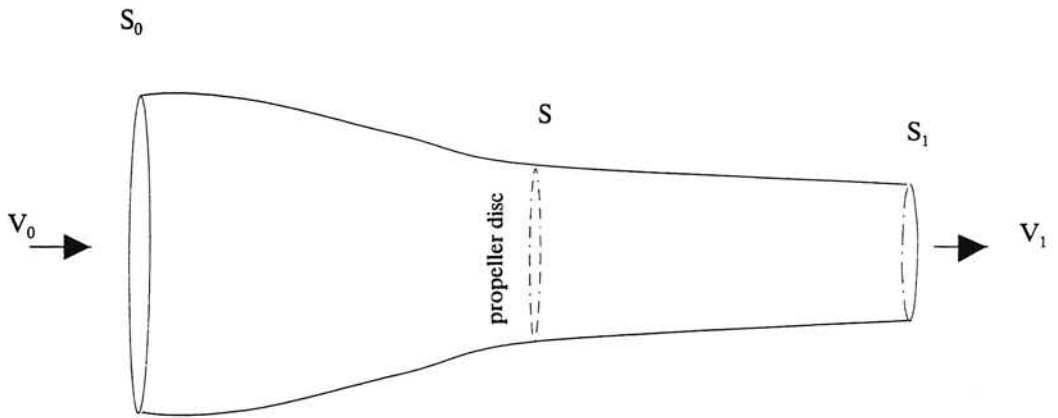


Fig 2.9 Propeller model in the axial momentum theory

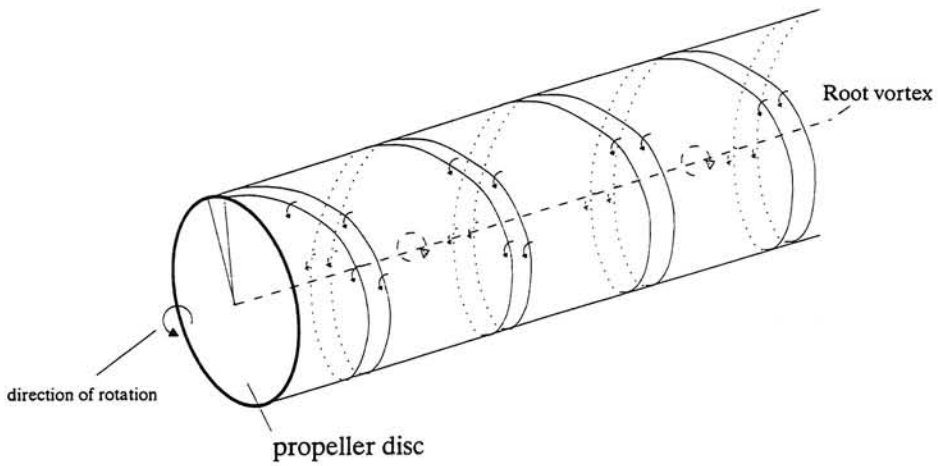


Fig 2.10 Wake model in Betz's vortex theory (infinite number of lightly loaded blades)

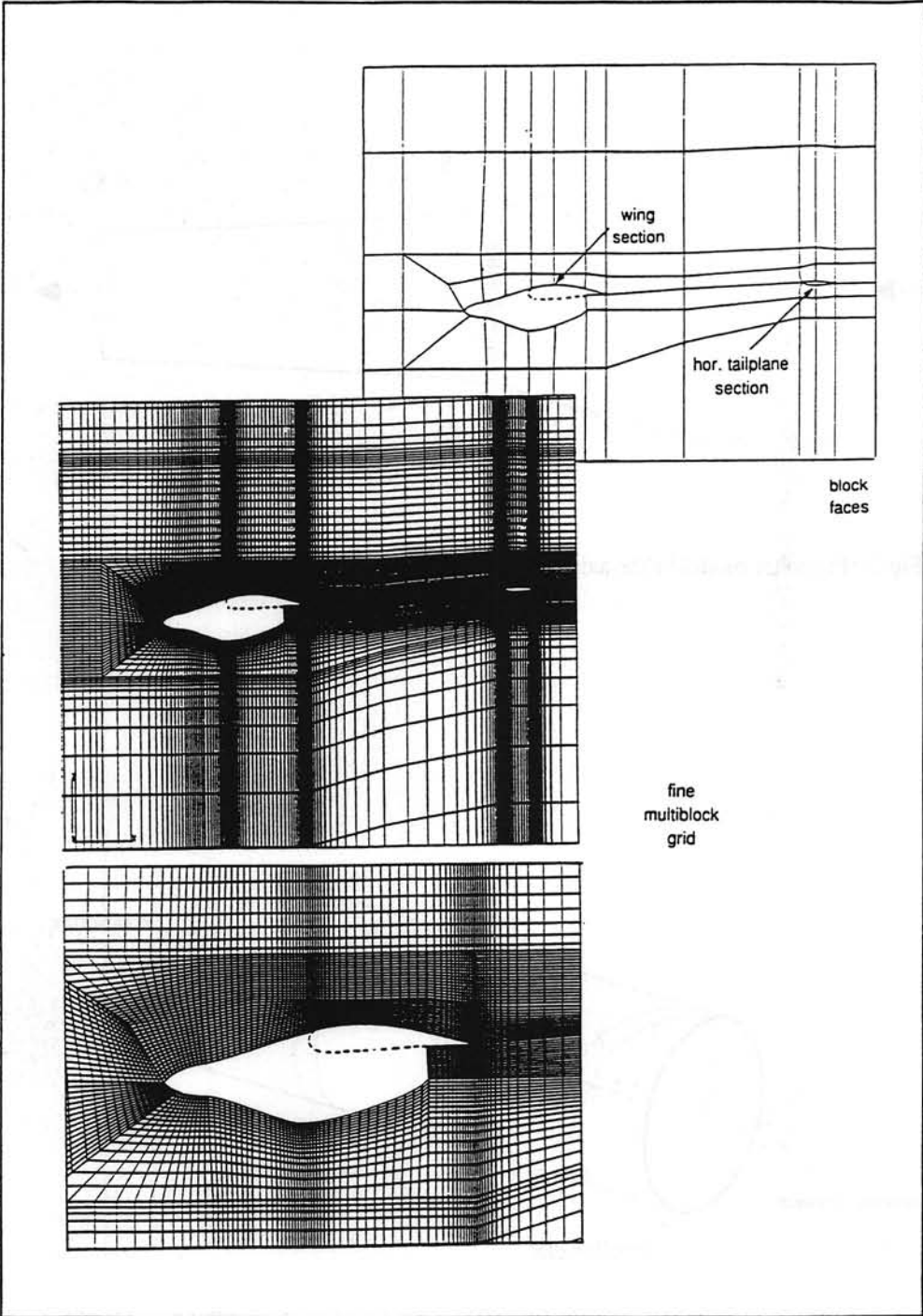
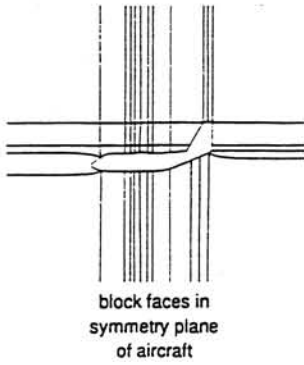


Fig 3.1
68

3-D finite volume grid around an aircraft configuration
(Boerstoeel [3.1])



fine multiblock
grid in flow

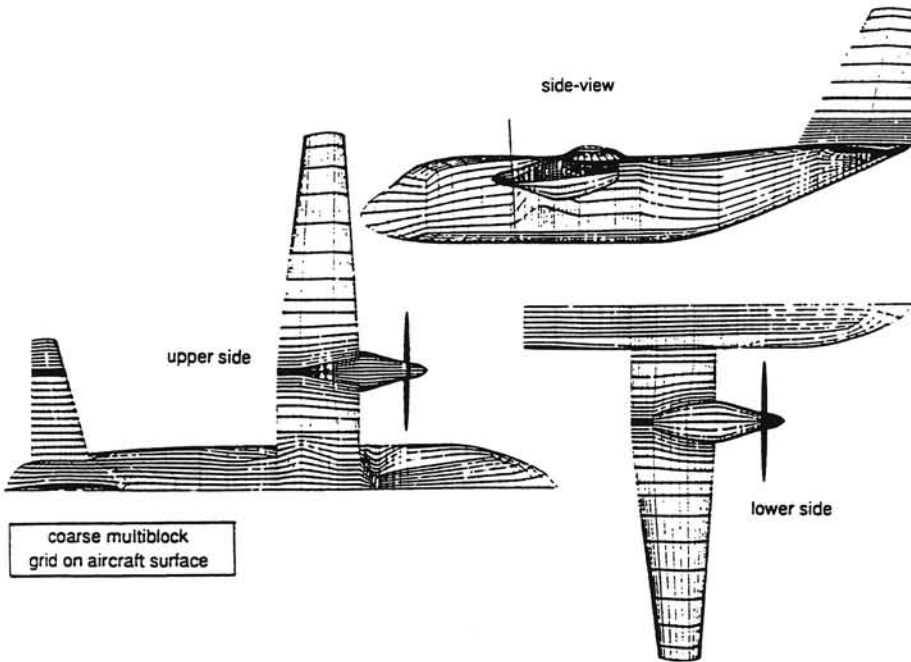
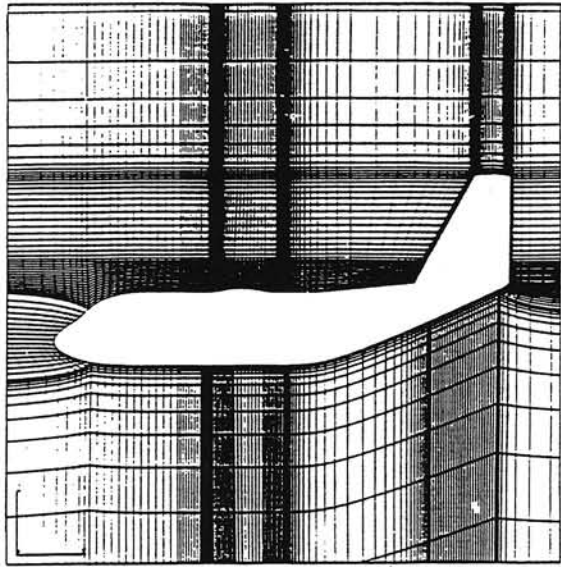


Fig 3.1 (Continued)

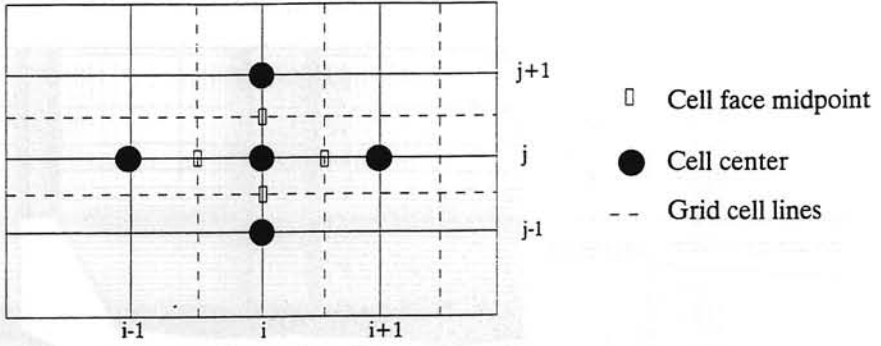


fig 3.2 'central' differencing scheme

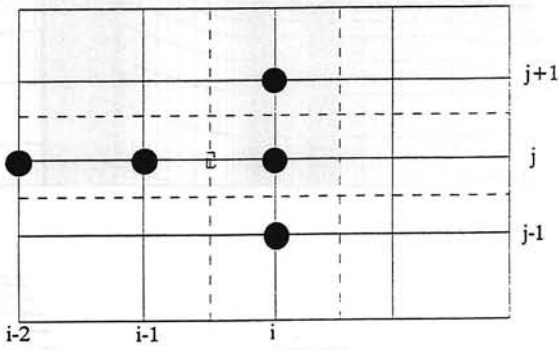


fig 3.3 'upwind' scheme in x-direction

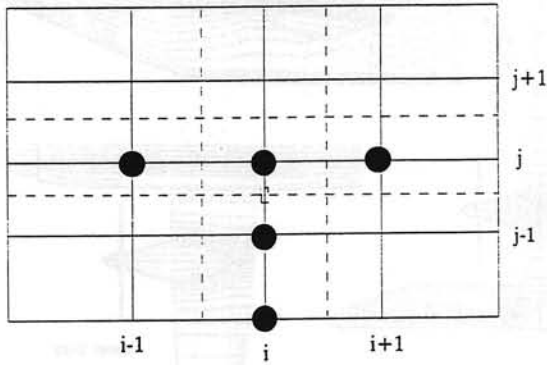


fig 3.4 'upwind' scheme in y-direction

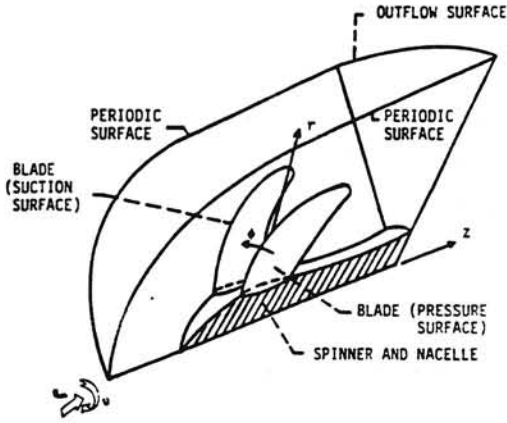


Fig 4.1.a The physical domain

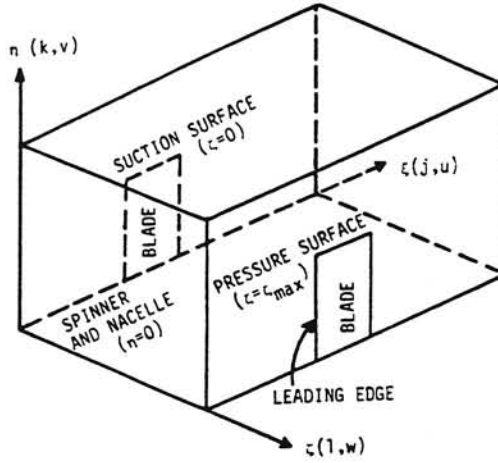


Fig 4.1.b The computational domain

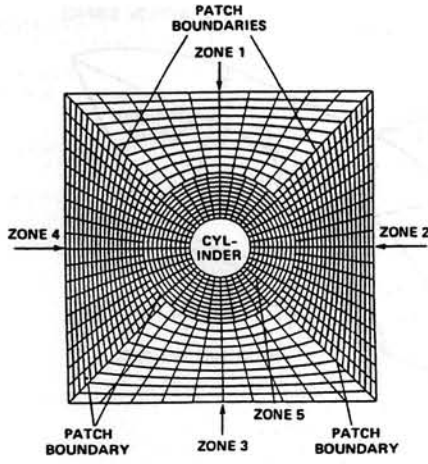


Fig 4.2 The patched grid approach

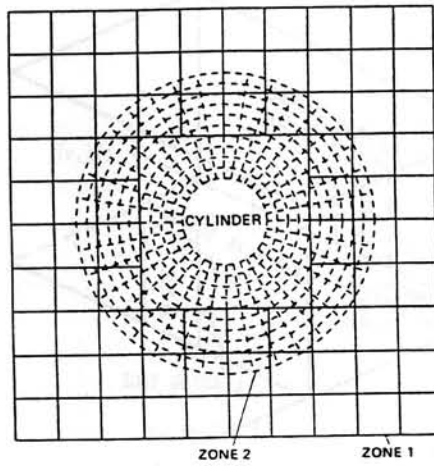


Fig 4.3 The overlaid grid approach

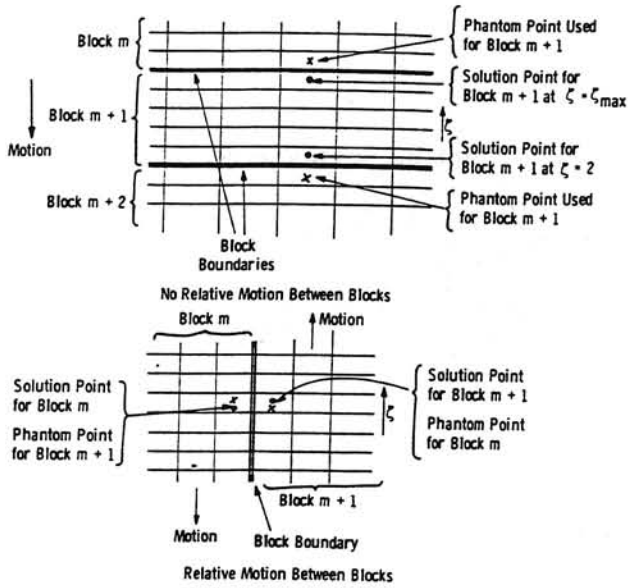


Fig 4.4 Definition of phantom points for moving grid blocks (Whitfield [4.6])

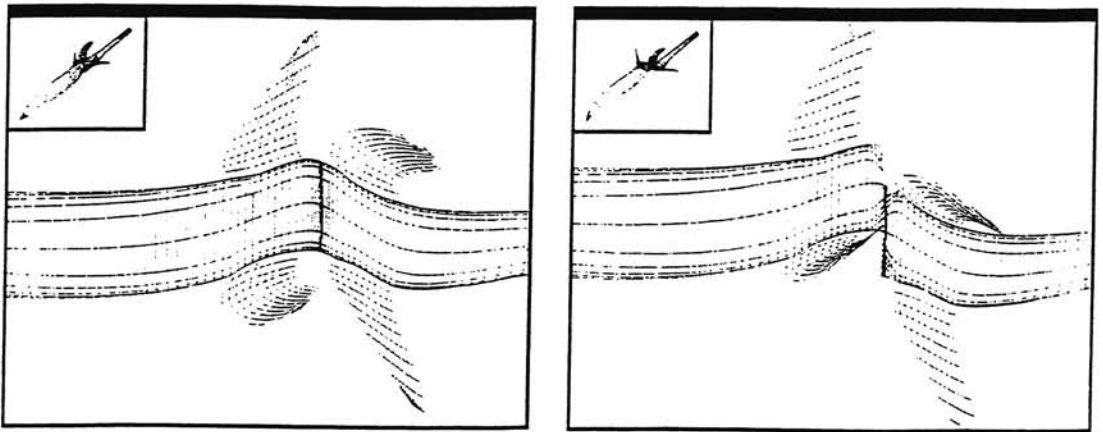


Fig 4.5 Localized grid-distortion for a counter-rotating propeller configuration
 a) The initial grid b) The distorted grid (Janus, Whitfield [4.7])

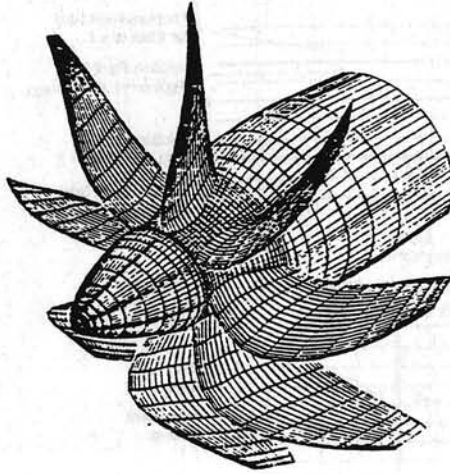


Fig 4.6 The Hamilton Standard SR-3 propeller (Yamamoto, Barton [4.3])

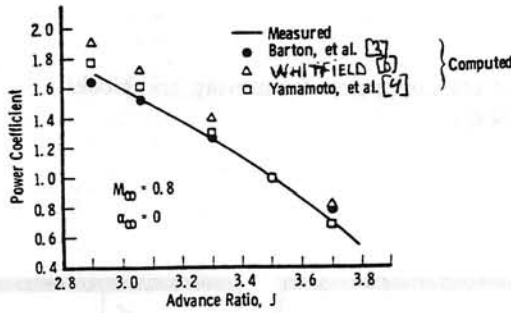


Fig 4.7 Power coefficients (calculated and experimental) (Whitfield [4.6])

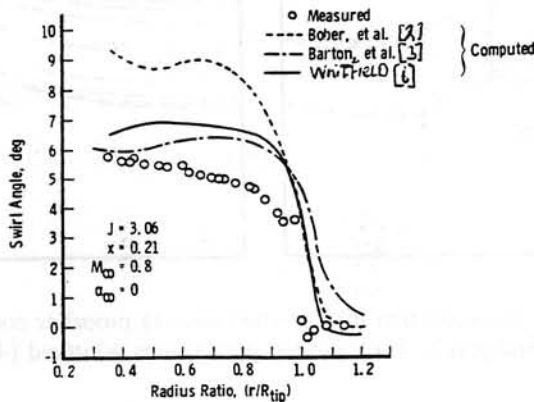


Fig 4.8 Swirl angle (calculated and experimental) (Whitfield [4.6])



Fig 4.9 The General Electric UnDucted Fan (Whitfield [4.6])

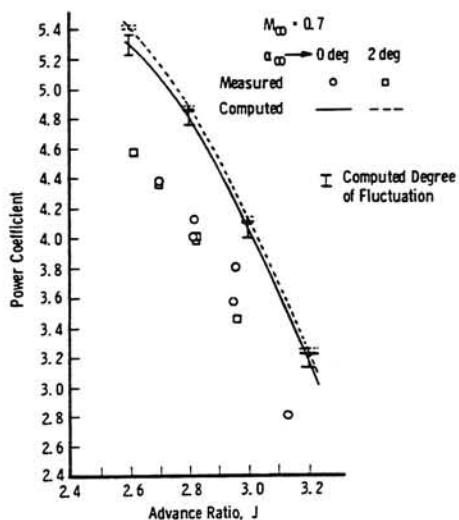


Fig 4.10 Power coefficients (calculated and experimental) (Whitfield [4.6])

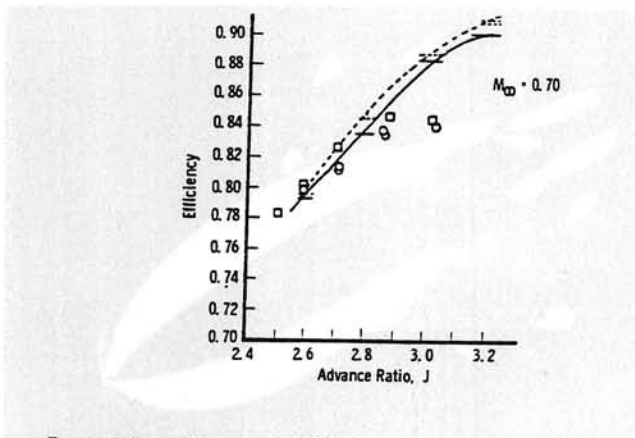


Fig 4.11 Propulsion efficiency (calculated and experimental) (Whitfield [4.6])

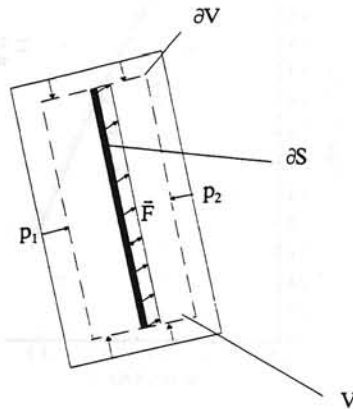


Fig 5.1.a Pressure and distributed force on elementary volume V bounded by edge ∂V intersected by actuator disc part ∂S (1=upstream side, 2=downstream side)

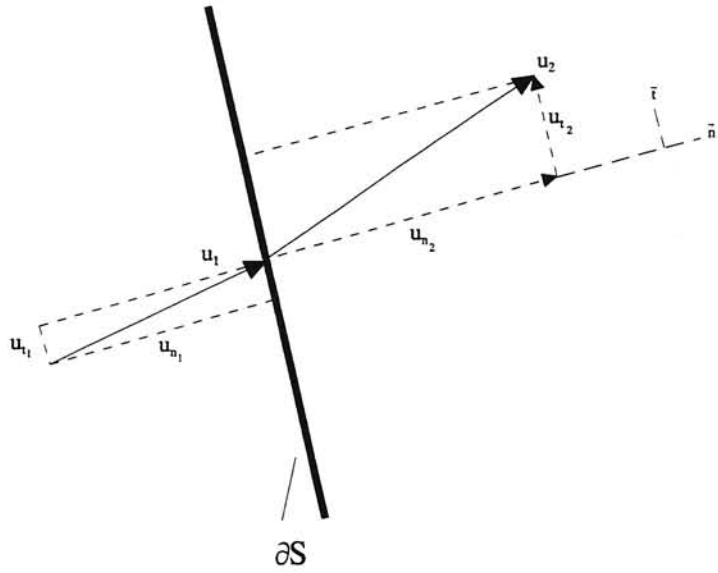


Fig 5.1.b Flow velocity components normal and tangential to the actuator disc part ∂S at the upstream and downstream side of the disc.



Figure 1. A diagram illustrating the relationship between the vertical axis and the horizontal axis. The vertical axis is labeled 'Y' and the horizontal axis is labeled 'X'. The diagram shows a vertical line with several horizontal lines extending to the left, representing different levels or states. The top horizontal line has an arrow pointing to the left, indicating a direction of movement or flow.

The diagram illustrates the relationship between the vertical axis and the horizontal axis. The vertical axis is labeled 'Y' and the horizontal axis is labeled 'X'. The diagram shows a vertical line with several horizontal lines extending to the left, representing different levels or states. The top horizontal line has an arrow pointing to the left, indicating a direction of movement or flow.

The diagram illustrates the relationship between the vertical axis and the horizontal axis. The vertical axis is labeled 'Y' and the horizontal axis is labeled 'X'. The diagram shows a vertical line with several horizontal lines extending to the left, representing different levels or states. The top horizontal line has an arrow pointing to the left, indicating a direction of movement or flow.

The diagram illustrates the relationship between the vertical axis and the horizontal axis. The vertical axis is labeled 'Y' and the horizontal axis is labeled 'X'. The diagram shows a vertical line with several horizontal lines extending to the left, representing different levels or states. The top horizontal line has an arrow pointing to the left, indicating a direction of movement or flow.

Series 01: Aerodynamics

01. F. Motallebi, 'Prediction of Mean Flow Data for Adiabatic 2-D Compressible Turbulent Boundary Layers'
1997 / VI + 90 pages / ISBN 90-407-1564-5
02. P.E. Skåre, 'Flow Measurements for an Afterbody in a Vertical Wind Tunnel'
1997 / XIV + 98 pages / ISBN 90-407-1565-3
03. B.W. van Oudheusden, 'Investigation of Large-Amplitude 1-DOF Rotational Galloping'
1998 / IV + 100 pages / ISBN 90-407-1566-1
04. E.M. Houtman / W.J. Bannink / B.H. Timmerman, 'Experimental and Computational Study of a Blunt Cylinder-Flare Model in High Supersonic Flow'
1998 / VIII + 40 pages / ISBN 90-407-1567-X
05. G.J.D. Zondervan, 'A Review of Propeller Modelling Techniques Based on Euler Methods'
1998 / IV + 84 pages / ISBN 90-407-1568-8
06. M.J. Tummies / D.M. Passchier, 'Spectral Analysis of Individual Realization LDA Data'
1998 / VIII + 36 pages / ISBN 90-407-1569-6
07. P.J.J. Moeleker, 'Linear Temporal Stability Analysis'
1998 / VI + 74 pages / ISBN 90-407-1570-X
08. B.W. van Oudheusden, 'Galloping Behaviour of an Aeroelastic Oscillator with Two Degrees of Freedom'
1998 / IV + 128 pages / ISBN 90-407-1571-8
09. R. Mayer, 'Orientation on Quantitative IR-thermography in Wall-shear Stress Measurements'
1998 / XII + 108 pages / ISBN 90-407-1572-6
10. K.J.A. Westin / R.A.W.M. Henkes, 'Prediction of Bypass Transition with Differential Reynolds Stress Models'
1998 / VI + 78 pages / ISBN 90-407-1573-4
11. J.L.M. Nijholt, 'Design of a Michelson Interferometer for Quantitative Refraction Index Profile Measurements'
1998 / 60 pages / ISBN 90-407-1574-2
12. R.A.W.M. Henkes / J.L. van Ingen, 'Overview of Stability and Transition in External Aerodynamics'
1998 / IV + 48 pages / ISBN 90-407-1575-0
13. R.A.W.M. Henkes, 'Overview of Turbulence Models for External Aerodynamics'
1998 / IV + 40 pages / ISBN 90-407-1576-9

Series 02: Flight Mechanics

01. E. Obert, 'A Method for the Determination of the Effect of Propeller Slipstream on a Static Longitudinal Stability and Control of Multi-engined Aircraft'
1997 / IV + 276 pages / ISBN 90-407-1577-7
02. C. Bill / F. van Dalen / A. Rothwell, 'Aircraft Design and Analysis System (ADAS)'
1997 / X + 222 pages / ISBN 90-407-1578-5
03. E. Torenbeek, 'Optimum Cruise Performance of Subsonic Transport Aircraft'
1998 / X + 66 pages / ISBN 90-407-1579-3

Series 03: Control and Simulation

01. J.C. Gibson, 'The Definition, Understanding and Design of Aircraft Handling Qualities'
1997 / X + 162 pages / ISBN 90-407-1580-7
02. E.A. Lomonova, 'A System Look at Electromechanical Actuation for Primary Flight Control'
1997 / XIV + 110 pages / ISBN 90-407-1581-5
03. C.A.A.M. van der Linden, 'DASMAT-Delft University Aircraft Simulation Model and Analysis Tool. A Matlab/Simulink Environment for Flight Dynamics and Control Analysis'
1998 / XII + 220 pages / ISBN 90-407-1582-3

Series 05: Aerospace Structures and Computational Mechanics

01. A.J. van Eekelen, 'Review and Selection of Methods for Structural Reliability Analysis'
1997 / XIV + 50 pages / ISBN 90-407-1583-1
02. M.E. Heerschap, 'User's Manual for the Computer Program Cufus. Quick Design Procedure for a CUt-out in a FUSelage version 1.0'
1997 / VIII + 144 pages / ISBN 90-407-1584-X
03. C. Wohlever, 'A Preliminary Evaluation of the B2000 Nonlinear Shell Element Q8N.SM'
1998 / IV + 44 pages / ISBN 90-407-1585-8
04. L. Gunawan, 'Imperfections Measurements of a Perfect Shell with Specially Designed Equipment (UNIVIMP)'
1998 / VIII + 52 pages / ISBN 90-407-1586-6

Series 07: Aerospace Materials

01. A. Vašek / J. Schijve, 'Residual Strength of Cracked 7075 T6 Al-alloy Sheets under High Loading Rates'
1997 / VI + 70 pages / ISBN 90-407-1587-4
02. I. Kunes, 'FEM Modelling of Elastoplastic Stress and Strain Field in Centre-cracked Plate'
1997 / IV + 32 pages / ISBN 90-407-1588-2
03. K. Verolme, 'The Initial Buckling Behavior of Flat and Curved Fiber Metal Laminate Panels'
1998 / VIII + 60 pages / ISBN 90-407-1589-0
04. P.W.C. Provoó Kluit, 'A New Method of Impregnating PEI Sheets for the *In-Situ* Foaming of Sandwiches'
1998 / IV + 28 pages / ISBN 90-407-1590-4
05. A. Vlot / T. Soerjanto / I. Yeri / J.A. Schelling, 'Residual Thermal Stresses around Bonded Fibre Metal Laminate Repair Patches on an Aircraft Fuselage'
1998 / IV + 24 pages / ISBN 90-407-1591-2
06. A. Vlot, 'High Strain Rate Tests on Fibre Metal Laminates'
1998 / IV + 44 pages / ISBN 90-407-1592-0
07. S. Fawaz, 'Application of the Virtual Crack Closure Technique to Calculate Stress Intensity Factors for Through Cracks with an Oblique Elliptical Crack Front'
1998 / VIII + 56 pages / ISBN 90-407-1593-9
08. J. Schijve, 'Fatigue Specimens for Sheet and Plate Material'
1998 / VI + 18 pages / ISBN 90-407-1594-7

Series 08: Astrodynamics and Satellite Systems

01. E. Mooij, 'The Motion of a Vehicle in a Planetary Atmosphere'
1997 / XVI + 156 pages / ISBN 90-407-1595-5
02. G.A. Bartels, 'GPS-Antenna Phase Center Measurements Performed in an Anechoic Chamber'
1997 / X + 70 pages / ISBN 90-407-1596-3
03. E. Mooij, 'Linear Quadratic Regulator Design for an Unpowered, Winged Re-entry Vehicle'
1998 / X + 154 pages / ISBN 90-407-1597-1

3021866

Future generation civil aircraft will be powered by new, highly efficient propeller propulsion systems. New, advanced design tools like Euler methods will be needed in the design process of these aircraft. This report describes the application of Euler methods to the modelling of flowfields generated by propellers. An introduction is given in the general layout of propellers and the propeller slipstream. It is argued that Euler methods can treat a wider range of flow conditions than the classical propeller theories. The power of Euler methods lies in the fact that a separate wake model is not needed because their solution includes the propeller slipstream. Two different ways are described of modelling the propeller slipstream using Euler methods. These are the time-accurate approach that uses the real propeller geometry and the time-averaged approach using an actuator disc representation of the propeller. Both techniques and their specifics concerning the imposition of boundary conditions and the grid are described. The results of a few propeller calculations using Euler methods are described. Discrepancies between experiments and the simulations can often be traced back to the neglect of the physical viscosity and the quality of the grid. Research is still ongoing into further improving the mathematical flow models and using new concepts like grid adaption.

ISBN 90-407-1568-8



9 799040 715685

